Research Square

Preprints are preliminary reports that have not undergone peer review.
They should not be considered conclusive, used to inform clinical practice,
or referenced by the media as validated information.

PRMT3-mediated arginine methylation of YBX1 promotes tumorigenesis in glioblastoma

Ji Wang

neuro-wangji@hotmail.com

The First Affiliated Hospital of USTC, Division of Life Sciences and Medicine, University of Science and Technology of China https://orcid.org/0000-0002-2657-9132

Shiquan Shen

The Second Affiliated Hospital of Guangzhou Medical University

Dongshan Zhang

Honglong Zhou

second affiliated hospital of Nanchang University

Zongyu Xiao

affiliated hospital of Qinghai University

Tianran Chai

Xinzhi Wu

The First Affiliated Hospital of USTC, Division of Life Sciences and Medicine, University of Science and Technology of China

Minghui Zeng

The First Affiliated Hospital of USTC, Division of Life Sciences and Medicine, University of Science and Technology of China

Li Jia

The First Affiliated Hospital of USTC, Division of Life Sciences and Medicine, University of Science and Technology of China

Zheng Li

The First Affiliated Hospital of USTC, Division of Life Sciences and Medicine, University of Science and Technology of China

Songsong Lu

The First Affiliated Hospital of USTC, Division of Life Sciences and Medicine, University of Science and Technology of China

Yang Tu

The First Affiliated Hospital of USTC, Division of Life Sciences and Medicine, University of Science and Technology of China

Xuanzhi Wang

The First Affiliated Hospital of USTC, Division of Life Sciences and Medicine, University of Science and Technology of China

Haibo Wu

the First Affiliated Hospital of USTC, Division of Life Sciences and Medicine, University of Science and Technology of China https://orcid.org/0000-0003-0817-9191

Nan Peng

Division of Life Sciences and Medicine, University of Science and Technology of China

Fei Wang

The First Affiliated Hospital of USTC, Division of Life Sciences and Medicine, University of Science and Technology of China

---

Article

Keywords:

Posted Date: February 27th, 2026

DOI: https://doi.org/10.21203/rs.3.rs-8924648/v1

License: This work is licensed under a Creative Commons Attribution 4.0 International License. Read Full License

Additional Declarations: There is no duality of interest

Abstract

Glioblastoma (GBM) represents one of the most challenging tumor types to treat clinically, characterized by an exceedingly poor patient prognosis. This is primarily attributable to the ambiguous molecular mechanisms that hinder the advancement of targeted therapies. Here, PRMT3 is identified as a key driver of tumorigenesis in GBM. Bioinformatics and clinical data reveal that high expression of PRMT3 in glioma cells is closely correlated with poor patient prognosis. Functional experiments demonstrate that PRMT3 overexpression enhances the proliferative capacity of GBM cells. Mechanistically, PRMT3 interacts with Y-box binding protein 1 (YBX1), and catalyzes the arginine methylation of YBX1 protein at R69 within its cold-shock domain. Subsequently, it was found that methylated YBX1 binds to 5-methylcytosine (m5C)-modified E2F1 mRNA and stabilizes its transcription, significantly promoting the expression of E2F1. The resulting PRMT3-YBX1-E2F1 axis sustains high E2F1 protein levels, activates a proliferation-associated transcriptional program, and is essential for GBM cell proliferation *in vitro* and *in vivo*. Meanwhile, the PRMT3 inhibitor SGC707 and the non-methylated YBX1 peptide significantly inhibited the proliferation of GBM cells. Our findings underscore that PRMT3 stabilizes E2F1 transcription through methylation of YBX1 at R69, promoting GBM tumorigenesis, and highlight the PRMT3-YBX1-E2F1 axis as a potential therapeutic target for GBM treatment.

INTRODUCTION

Glioblastoma (GBM), as the most common and lethal primary malignant tumor of the central nervous system, is characterized by continuous proliferation and significant biological heterogeneity, posing a major and persistent therapeutic challenge [1]. The 2021 WHO Classification of Tumors of the Central Nervous System introduced an integrated histological-molecular framework that incorporates hallmark genomic alterations-including IDH1/2 mutations, 1p/19q codeletion, TERT promoter mutations, EGFR amplification and CDKN2A/B homozygous deletion-together with MGMT promoter methylation status, thereby markedly improving diagnostic and prognostic precision [2]. Among these, EGFR amplification and CDKN2A/B loss are established drivers of malignant proliferation, acting through constitutive activation of mitogenic signaling and abrogation of cell-cycle checkpoints, respectively [3]. However, these static genetic alterations alone cannot account for the remarkable adaptability and sustained proliferative capacity of glioma cells under therapeutic pressure and changing microenvironmental conditions. Increasing evidence indicates that, beyond the genome, dynamic regulatory mechanisms-encompassing epigenetic, transcriptional, post-transcriptional and post-translational layers-collectively orchestrate gene-expression programs without altering the underlying DNA sequence. Together, these mechanisms form highly interwoven regulatory networks that provide critical plasticity for tumor cells to maintain high proliferative states in complex microenvironments, thereby driving glioma progression [4]. Elucidating how these regulatory layers converge on and amplify proliferative signaling along defined molecular axes remains a central challenge in understanding glioma biology [5].

Protein arginine methylation, catalyzed by protein arginine methyltransferases (PRMTs), is a pivotal post-translational modification in cancer [6]. By methylating both histone and diverse non-histone substrates,

PRMTs modulate epigenetic states, transcription, RNA metabolism and oncogenic signaling, thereby occupying a nodal position at the intersection of epigenetic, transcriptional and post-transcriptional regulation. This multilayered control establishes PRMTs as central regulators of tumor initiation, progression, therapy resistance and immune evasion [7, 8]. PRMT3, a type I enzyme, is characterized by a unique N-terminal zinc-finger domain that confers substrate specificity towards RGG/RG motifs, enabling it to catalyze the formation of asymmetric dimethylarginine (aDMA) on target proteins, and was initially identified as a regulator of ribosome biogenesis and translation [9]. More recently, PRMT3 has been shown to exert oncogenic functions in multiple solid tumors [10]. It enhances tumor-cell proliferation and metastasis by promoting aDMA of histone H4 at arginine 3 (H4R3me2a) and modulating endoplasmic reticulum (ER) stress signaling [11]; it methylates the transcription factor TFAP2A to augment its binding to the IDO1 promoter, thereby driving kynurenine synthesis and mediating radioresistance and immune evasion [12]; and it methylates RNA-binding proteins such as IGF2BP1 and the m6A-associated methyltransferase METTL14, stabilizing oncogenic transcripts, regulating GPX4 expression and influencing ferroptosis susceptibility [13, 14]. In colorectal cancer, PRMT3 promotes tumorigenesis by methylating and stabilizing HIF1α [15]. In glioma, PRMT3 is likewise upregulated and has been reported to promote glioma progression by enhancing HIF1α-dependent glycolysis and metabolic reprogramming [16]. However, whether PRMT3 directly drives malignant proliferation in glioma cells, and which substrates and downstream pathways mediate such effects, remains poorly understood.

Y-box binding protein 1 (YBX1), a member of the cold-shock protein family, serves as a validated m5C “reader” that recognizes 5-methylcytosine (m5C) modifications on mRNA deposited by NOP2/Sun domain (NSUN) family RNA methyltransferases or DNA methyltransferase 2 (DNMT2), thereby regulating the stability and fate of target transcripts [17]. YBX1 is highly expressed in a wide range of malignancies as a result of transcriptional upregulation and reduced protein degradation, and its overexpression is closely associated with tumor progression, chemoresistance and poor clinical outcome [18]. In addition, YBX1 itself is subject to intricate regulation by multiple post-translational modifications, including phosphorylation, ubiquitination and acetylation, which alter its subcellular localization, RNA-binding repertoire and protein–protein interaction networks, thereby contributing to tumor evolution [19]. Also, YBX1 is significantly upregulated in gliomas and could promote the growth of tumor cells. Mechanistically, the phosphorylation-dependent nuclear translocation of YBX1 enhances DNA damage repair and inhibits tumor cell apoptosis [20]. However, whether arginine methylation contributes to the regulation of YBX1 activity in glioma remains unknown.

Here, we demonstrate that PRMT3 is highly expressed in GBM and directly methylates YBX1 at arginine 69 within its cold-shock domain. This modification facilitates the binding of YBX1 to E2F1 mRNA, thereby enhancing the stability of E2F1 transcripts. The resulting PRMT3-YBX1-E2F1 axis sustains high E2F1 protein levels, activates a proliferation-associated transcriptional program, and is essential for GBM cell proliferation *in vitro* and *in vivo*. These findings identify arginine methylation as a previously unrecognized post-transcriptional regulatory “switch” in GBM that links epigenetic reprogramming to cell-

cycle dysregulation, and establish the PRMT3-YBX1-E2F1 axis as a therapeutically actionable vulnerability in GBM.

RESULTS

PRMT3 is overexpressed in glioma and correlates with poor prognosis

To understand the expression profiles of PRMT3 in tumor, pan-cancer analysis was performed to detect its expression patterns across all tumor types. When comparing expression levels across all tumor tissues, PRMT3 exhibited the highest expression in glioma (including LGG and GBM) among all cancer types (Fig. 1A). Moreover, PRMT3 showed significant overexpression in gliomas when compared with normal tissues (Fig. 1B). To further resolve PRMT3 expression across distinct cellular compartments within the tumor microenvironment, we integrated single-cell RNA sequencing (scRNA-seq) data from three distinct cohorts (GSE102130, GSE70630, and GSE131928). This integrated analysis demonstrates that PRMT3 is predominantly expressed in malignant cell populations, including AC-like malignant cells, OC-like malignant cells, OPC-like malignant cells, and oligodendrocytes, with its expression levels being significantly higher compared to immune cells or endothelial cells (Fig. 1C-I). Subsequently, we validated the expression and clinical significance of PRMT3 in the Rembrandt dataset (a renowned clinical glioma cohort). The expression profile of PRMT3 in tissue samples demonstrated significantly higher PRMT3 expression in gliomas compared to Non tumor brain tissues (Fig. 1J). The significance of upregulated PRMT3 expression in glioma patient prognosis indicates that patients with higher PRMT3 expression levels in glioma or GBM have worse overall survival compared to those with lower PRMT3 expression (Fig. 1K, L). Furthermore, receiver operating characteristic (ROC) curve analysis demonstrated robust diagnostic accuracy, with an area under the curve (AUC) of 0.977, indicating that PRMT3 holds significant prognostic diagnostic value for glioma (Fig. 1M). In addition, we collected a portion of freshly glioma samples and immunohistochemical (IHC) results showed that compared to Non tumor brain tissues, the PRMT3 protein levels were significantly elevated, particularly in GBMs (Fig. 1N, O). These findings collectively establish PRMT3 overexpression as a key contributor to poor prognosis in glioma.

PRMT3 drives malignant proliferation in GBM

To investigate the functional role of PRMT3 in GBM, we generated stable PRMT3 knockdown and overexpression models in U87 and T98 cell lines by shRNA or ORF plasmids, verifying efficient modulation of PRMT3 expression by RT-qPCR and western blotting (Fig. 2A-D). Then, CCK-8 assays demonstrated that PRMT3 silencing significantly attenuated cellular proliferation in both U87 and T98 cells, while reintroduction of PRMT3 in knockdown cells effectively restored growth (Fig. 2E). These findings were further corroborated by colony formation assays, wherein PRMT3 depletion strongly suppressed colony formation, while reconstitution restored the proliferative ability of GBM cells (Fig. 2F, G). Pharmacological inhibition of PRMT3 with SGC707, at concentrations exceeding 100 μM,

recapitulated the results from genetic knockdown by producing a concentration-dependent suppression of GBM cell proliferation (Fig. 2H-J). Furthermore, *in vivo* experimental validation demonstrated that xenograft models generated by PRMT3-silenced U87 cells exhibited slower tumor growth and significantly prolonged overall survival time compared with control groups (Fig. 2K-M). IHC analysis of xenograft tumor tissues revealed a significant decrease in the Ki67 labeling index in PRMT3-deficient tumors. EGFR and its downstream RAS/ERK and PI3K/AKT signaling pathways have been confirmed as the most critical signaling pathways driving tumor cell proliferation [21]. Therefore, we examined the association between PRMT3 and these signaling pathways in GBM cells, and the immunoblotting results showed PRMT3 overexpression promoted EGFR phosphorylation at Tyr1068 and activated downstream RAS/ERK and PI3K/AKT pathways (Fig. 2P-R). Together, targeting PRMT3 through genetic and pharmacological approaches could inhibit the proliferative effects of GBM cells both *in vivo* and *in vitro*, thereby confirming that PRMT3 is a critical factor mediating the malignant progression of GBM.

PRMT3 mediates arginine methylation of YBX1

To investigate the mechanism by which PRMT3 promotes GBM progression, we immunoprecipitated PRMT3 recombinant proteins from U87, T98, and PRMT3-overexpressing HEK293T cells, followed by analysis using liquid chromatography-tandem mass spectrometry (LC-MS/MS). We identified 272 PRMT3-interacting proteins that overlapped between these three cells (Fig. 3A). It is noteworthy that YBX1 (a DNA/RNA-binding protein that drives cell proliferation, tumor progression, and multidrug resistance by regulating cancer-associated gene networks [18]) is one of the proteins with the highest abundance immunoprecipitated by PRMT3. To validate our IP-MS findings, we examined whether YBX1 interacted with PRMT3. First, immunofluorescence assays revealed their cytoplasmic co-localization in U87 and T98 cells (Fig. 3B). Then, we examined whether YBX1 interacts with PRMT3 at both endogenous and exogenous levels. Indeed, we found that endogenous PRMT3 effectively precipitated endogenous YBX1 in U87 and T98 cells, and YBX1-HA was detected in the precipitates with exogenous PRMT3-FLAG in HEK293T cells (Fig. 3C and Supplementary Fig. 1A, B). Given that PRMT3 and YBX1 have been verified to play transcriptional regulatory roles in tumor cells [10, 18], we therefore investigated whether there exists a transcriptional regulatory mechanism between them. In GBM cells with PRMT3 knockdown or inhibition of PRMT3 protein activity, we did not detect any changes in YBX1 expression at the transcriptional level (Supplementary Fig. 2A, B). Also, the total protein abundance of YBX1 and the phosphorylation level at Ser102 site were not altered by the silencing or inhibition of PRMT3 (Supplementary Fig. 2C, D). Similarly, no effects were observed on the transcriptional level of YBX1 or the phosphorylation level at Ser102 in GBM cells following PRMT3 overexpression (Supplementary Fig. 2E, F). On the other hand, no changes in PRMT3 protein and RNA expression levels were observed in GBM cells with silencing or overexpressing YBX1 (Supplementary Fig. 2G-K), indicating their interaction does not involve transcriptional or translational regulation. Given that PRMT3 functions through its arginine methyltransferase activity [13, 14], we investigated whether it could catalyze arginine methylation of YBX1. In GBM cells, silencing PRMT3 significantly reduced the overall asymmetric dimethylarginine (aDMA) levels, while overexpression of PRMT3 increased aDMA levels. Interestingly, the most prominent

aDMA signal detected by western blotting appeared at the molecular weight corresponding to YBX1 (Supplementary Fig. 3A, B). Further, we detected the aDMA signal of YBX1 in the precipitates of exogenous PRMT3-FLAG or YBX1-HA (Fig. 3D, E), indicating that PRMT3 could mediate arginine methylation modification of YBX1. To directly assess the regulation of endogenous YBX1 arginine methylation levels by PRMT3, we first evaluated the presence of arginine methylation modifications on YBX1 protein in U87 and T98 cells. Compared with control cells, the level of aDMA on immunoprecipitated YBX1 protein significantly decreased in GBM cells treated with the methyltransferase inhibitor Adenosine dialdehyde (AdOx), indicating that YBX1 protein undergoes arginine methylation modification in GBM cells (Supplementary Fig. 4A). Moreover, we performed co-immunoprecipitation experiments in U87 and T98 cells with PRMT3 knockdown or treatment with the inhibitors SGC707, substantially reduced YBX1-aDMA levels (Fig. 3F, G). Conversely, overexpression of PRMT3 enhanced arginine methylation of the YBX1 protein, whereas the PRMT3 mutant (E338Q) failed to catalyze the methylation modification of YBX1 protein compared to wild-type PRMT3 (Fig. 3H, I). Collectively, these results demonstrate that PRMT3 interacts with YBX1 in GBM cells and catalyzes asymmetric dimethylation modification on arginine residues of the YBX1 protein.

PRMT3 methylates YBX1 at R69

To identify the methylation sites of YBX1 protein catalyzed by PRMT3, we used the AlphaFold3 tool for prediction, with the R69 and R101 sites demonstrating the highest binding scores (Fig. 4A). R69 or R101 is the presumed methylation site of YBX1, and the amino acid regions surrounding R69 and R101 in the YBX1 protein sequence are highly conserved across multiple species (Fig. 4C). Next, to further identify the specific binding sites of PRMT3 on the YBX1 protein, we constructed eight HA-tagged YBX1 truncations, including deletion variants of the cold shock domain (CSD) (either complete or partial deletions) or arginine-to-lysine mutants at position 69 or position 101 (R-to-K) (Fig. 4B, C). Notably, in HEK293T cells, deletion of the CSD (Δ52–129) region (and to a lesser extent the CSD (Δ61–70) region) significantly blocked the interaction between PRMT3 and YBX1 (Fig. 4D). Consistent with this, in U87 cells, deletion of either the CSD (Δ52–129) region or the CSD (Δ61–70) region nearly completely abolished the intracellular interaction between the two proteins (Fig. 4E). We co-transfected PRMT3 plasmid with either YBX1 R69K mutant or YBX1 R101K mutant in 293T cells and performed Co-IP experiments. The results showed that PRMT3 could not Co-immunoprecipitate with the YBX1 R69K mutant, but still bound to the R101K mutant, thereby identifying Arg69 as the critical contact site and methylation-accepting residue (Fig. 4F). To determine whether endogenous YBX1 undergoes dimethylation modification in GBM cells, we synthesized peptides containing asymmetrically dimethylated R69 and used it as an antigen to prepare rabbit-derived polyclonal antibodies, which specifically recognize dimethylated YBX1 protein. Subsequently, we used this antibody to detect endogenous methylated YBX1 protein in GBM cells. Western blotting results showed that only a weak YBX1 methylation signal could be detected in PRMT3-KD cells compared to control GBM cells, whereas the YBX1 methylation signal was remarkably prominent in PRMT3-overexpressing cells (Fig. 4G, H). Similarly, the asymmetric dimethylarginine modification of YBX1-R69 can be eliminated by using either

the PRMT3 inhibitor (SGC707) or the arginine methylation inhibitor (AdOx) (Fig. 4I). Moreover, the R69K mutant showed obvious reduced level of R69 asymmetric dimethylation in comparison with WT (Fig. 4J). Consistent with our observations in Fig. 4K, L, PRMT3 siRNA treatment inhibited asymmetric dimethylation of R69 in U87 and T98 cells. Then, we re-expressed PRMT3 in GBM cells with stable PRMT3 knockdown and found that it could effectively restore the methylation level of YBX1-R69 (Fig. 4M, N). In 293T cells, exogenously overexpressed PRMT3 can significantly promote the methylation of exogenous YBX1-R69, while it has no obvious effect on the methylation level of exogenous YBX1-R69K (Fig. 4O). Collectively, these data demonstrated that PRMT3 directly promotes arginine methylation of YBX1 at R69 in GBM cells.

PRMT3-mediated asymmetric dimethylation of YBX1 at R69 is required for GBM cell growth

We next investigated whether R69 asymmetric dimethylation of YBX1 plays a role in GBM cell. First, western blotting results indicated that YBX1-knockout (YBX1-KO) GBM cell lines were generated and then rescued with wild-type YBX1 (YBX1-WT) or methylation-deficient mutant (YBX1-R69K) (Fig. 5A). As shown in Fig. 5B, C and Supplementary Fig. 5A, YBX1 knockout led to weakened GBM cell proliferation, which was significantly restored upon re-expression of YBX1-WT. However, when the R69K mutant of YBX1 was reintroduced, the weakened cell growth was not markedly reversed. To validate these observations, we established an intracranial xenograft mouse model by implanting YBX1-KO cells and YBX1-KO U87 cells rescued with YBX1-WT or R69K mutant into the brains of BALB/c nude mice. By measuring tumor size and monitoring the survival prognosis of tumor-bearing mice, we found that YBX1-KO significantly inhibited tumor growth and prolonged survival, while YBX1-WT rescue restored tumor growth and survival. Notably, re-expression of R69K barely rescued tumor growth or prognosis (Fig. 5D, E, H). In addition, the inhibition of tumor growth was accompanied by a significant reduction in Ki67 expression and YBX1-R69 methylation in tumor cells (Fig. 5F, G). These results demonstrate that YBX1 asymmetric dimethylation at R69 facilitates the growth and proliferation of GBM cells *in vitro* and *in vivo*.

Furthermore, we investigated whether YBX1 methylation could serve as a therapeutic target for GBM. We synthesized a competitive non-methylated YBX1 peptide containing the R69 methylation site, with the N-terminal region labeled with the transcription trans-activator (TAT) peptide. Methylated peptide corresponding to the R69 site and untreated groups were used as negative controls (Fig. 5I). The Co-IP results indicated that the non-methylated peptide (rather than the methylated peptide) significantly inhibited the methylation of the R69 site of YBX1 in GBM cells (Fig. 5J), and both the methylated or nonmethylated peptides had no obvious effect on the interaction between PRMT3 and YBX1 (Fig. 5K and Supplementary Fig. 6A, B). Then, we examined the effect of synthetic peptides on GBM cell proliferation. The data showed that cells treated with non-methylated peptides exhibited suppressed GBM cell proliferation compared to those treated with methylated peptides (Fig. 5L-N). To explore *in vivo* antitumor effects of non-methylated peptides, we established a subcutaneous xenograft mouse model. As shown in Fig. 5O, Q, treatment with non-methylated peptides almost completely inhibited the growth

of subcutaneous GBM, while methylated peptides exhibited no such effect. The expression of Ki67 in tumors also reflected the inhibitory effect of non-methylated peptides on tumor cells (Fig. 5P, R). Therefore, these findings suggest that targeting YBX1 methylation may serve as a potential therapeutic strategy for GBM treatment.

E2F1 is identified as a key downstream target of the PRMT3-YBX1 axis

To map the downstream regulatory network of the PRMT3-YBX1 axis, we employed a multi-omics screening strategy. Initially, we analyzed the data of RNA-seq in PRMT3-KD and YBX1-KD GBM cells, with the results visualized by volcano plots (Fig. 6A, B). Screening of commonly downregulated genes revealed that 12 shared genes exhibited suppressed expression in both PRMT3-KD and YBX1-KD GBM cells (Fig. 6C). Given the central role of YBX1 as a DNA- and RNA-binding protein, we integrated YBX1 eCLIP (enhanced ultraviolet (UV) cross-linking and immunoprecipitation) sequencing data in U251 cells to identify its direct binding sites [22]. We combined the results from RNA-seq and eCLIP-seq, and found 11 candidate genes associated with PRMT3/YBX1 in GBM cells. Subsequently, GO enrichment analysis of PRMT3-KD data revealed significant enrichment of cell cycle and proliferation-related processes, and we searched the literature for the functions of these 11 candidate genes (Fig. 6D and Supplementary Fig. 7). E2F1 has been verified as a key regulator of tumor cell cycle and proliferation [22, 23]. Collectively, the above information indicates that E2F1 could be direct targets of YBX1 which is related to GBM cell proliferation. To test this hypothesis, RT-qPCR analysis results showed that knockdown of PRMT3, pharmacological inhibition of PRMT3 with SGC707, or knockdown of YBX1 significantly reduced E2F1 mRNA levels in GBM cells (Fig. 6E, I and Supplementary Fig. 8A). Conversely, overexpression of PRMT3 or YBX1 increased E2F1 mRNA levels (Fig. 6F, J). In line with those data, western blotting demonstrated that knockdown or inhibition of PRMT3, or knockdown of YBX1, decreased E2F1 protein levels, whereas overexpression of PRMT3 or YBX1 increased E2F1 protein expression (Fig. 6G, K, H, L and Supplementary Fig. 8B). Together, these findings demonstrate that PRMT3 and YBX1 positively regulate E2F1 transcription, and identify E2F1 as a downstream target of the PRMT3-YBX1 signaling axis.

PRMT3-YBX1 axis enhances the stabilization of m5C-modified E2F1 mRNA

Given our finding that the PRMT3-YBX1 axis upregulates E2F1 transcription, we investigated the mechanism by which PRMT3-YBX1 regulates E2F1 expression. YBX1 is widely recognized as an m5C “reader” that regulates mRNA stability, thereby modulating gene expression and influencing disease progression [17]. We conducted further analysis of the eCLIP-seq data for YBX1 binding sites in U251 cells. Motif enrichment analysis based on high-ranking YBX1 binding sites revealed that the most enriched 4-base and 8-base motifs were CAUC and UUACCAUC (known core RNA-binding motifs of YBX1), respectively (Fig. 7A). Additionally, peaks corresponding to E2F1 mRNA were identified in the

RNA precipitated by YBX1 antibody (Fig. 7B). We performed RIP-qPCR experiments to confirm the binding of E2F1 mRNA to YBX1 protein in GBM cells (Fig. 7C). Then, we observed that depletion of PRMT3 in GBM cells reduced the binding of YBX1 to E2F1 mRNA (Fig. 7D), while overexpression of PRMT3 increased the binding of YBX1 to E2F1 mRNA. Interestingly, no significant change was observed in the binding of YBX1 to E2F1 mRNA after overexpression of PRMT3 mutants (Fig. 7D), suggesting that PRMT3 promotes the binding of YBX1 to E2F1 mRNA. To assess the effect of PRMT3 or YBX1 expression on E2F1 mRNA stability, we treated GBM cells with actinomycin D to block transcription and monitored the decay kinetics of E2F1 mRNA by RT-qPCR. We found that knockdown of PRMT3 or YBX1 expression accelerated the degradation of E2F1 mRNA, while overexpression of PRMT3 or YBX1 prolonged the half-life of E2F1 mRNA (Fig. 7F-I). Supporting clinical relevance, YBX1 showed a significant positive correlation with E2F1 in the CGGA glioma dataset (Fig. 7J). Therefore, these data indicated that the PRMT3-YBX1 axis may promote E2F1 expression by enhancing its mRNA stability. Since YBX1 preferentially binds m5C-modified transcripts, we investigated whether the m5C methyltransferase NSUN2 cooperates with the PRMT3-YBX1 axis. Indeed, RT-qPCR and western blotting results demonstrated that NSUN2 expression in GBM cells promotes E2F1 transcription (Fig. 7K-N). In addition, YBX1 RIP-qPCR and E2F1 RNA decay assays revealed that NSUN2 enhances YBX1's recognition of E2F1 mRNA and increases its RNA stability (Fig. 7O-R). Similarly, we also observed a positive correlation between the expression of NSUN2 and E2F1 in clinical specimens (Fig. 7S). Collectively, these findings demonstrate that PRMT3-YBX1 axis could maintain the stability of E2F1 mRNA in GBM cells via NSUN2-mediated m5C modification.

The effect of PRMT3-YBX1 on GBM cell proliferation is dependent on E2F1

E2F1 is a core transcription factor that sustains growth in tumor cells, and is also a key regulator known to control cell cycle progression, apoptosis, as well as the expression of multiple cell growth factors and cytokines [22, 23]. In the E2F1 knockdown or overexpression GBM cell models we established (Fig. 8A-D), it was observed that the loss of E2F1 led to decreased cell proliferation capacity, while increased E2F1 expression showed the opposite growth trend (Fig. 8E-H). To further confirm that the PRMT3-catalyzed asymmetric dimethylation of YBX1 at R69 regulates E2F1 expression, we co-expressed PRMT3-FLAG and YBX1-HA (WT or R69K) in GBM cells with PRMT3-KD. The RT-qPCR and western blotting data revealed that PRMT3 overexpression increased E2F1 expression levels in cells expressing YBX1-WT but not the YBX1-R69 mutation (Fig. 8I, J), suggesting that PRMT3-mediated arginine methylation of YBX1 plays an important role in regulating E2F1 expression. Moreover, we found that the proliferative effect of GBM cells induced by PRMT3 overexpression was reversed after YBX1 silencing (Fig. 8K-M and Supplementary Fig. 9A). Since E2F1 is regulated by PRMT3, we examined whether E2F1 functions as a downstream effector of PRMT3 to regulate GBM cell proliferation. We re-expressed E2F1 in PRMT3-silenced GBM cells (Fig. 8N) and found that E2F1 overexpression could rescue the effects of PRMT3 knockdown on GBM cell proliferation (Fig. 8O and Supplementary Fig. 9B). Also, we observed that knockdown of E2F1 abolished the effect of PRMT3 overexpression on GBM cell proliferation, leading

to decreased cell proliferative capacity (Fig. 8P-R and Supplementary Fig. 9C). Together, our results establish E2F1 as a key downstream effector of PRMT3-dependent YBX1 methylation in GBM cells.

YBX1 is hypermethylated by PRMT3 at R69 in human glioma tissues and predicts poor patient prognosis

Given that we have confirmed through *in vitro* and *in vivo* experiments that PRMT3 could catalyze the asymmetric dimethylation of arginine at R69 of the YBX1 protein, thereby enhancing the m5C modification of E2F1 mRNA mediated by NSUN2 to stabilize the transcript and increase its expression. Next, we evaluated the clinical relevance of the PRMT3-YBX1-E2F1 axis by clinical specimens from glioma patients. IHC analysis revealed significantly higher levels of YBX1-R69me2a in tumor tissues compared with non-tumor tissues. Notably, its staining intensity positively correlated with histological grade, showing stronger signals in high-grade glioma and GBM (Fig. 9A, B). Based on the expression data of PRMT3 in clinical glioma cohorts, we found a significant positive correlation between PRMT3 and YBX1-R69me2a expression in the same samples (Fig. 9C, D). Furthermore, consistent with our observations, western blotting demonstrated that PRMT3, YBX1, YBX1-R69me2a, E2F1 and NSUN2 protein expression were all increased in glioma tissues compared with non-tumor controls (Fig. 9E). The expression correlation analysis results showed that PRMT3 expression was significantly positively associated with both YBX1-R69me2a and E2F1 levels, and that YBX1 protein levels also positively correlated with E2F1 expression (Fig. 9F-H). Importantly, aberrant activation of this pathway was linked to poor clinical outcome. Kaplan-Meier survival analysis revealed that patients with high PRMT3 expression or high YBX1-R69me2a levels had significantly shorter overall survival than those with low expression of these markers (Fig. 9I, J). Taken together, our clinical data demonstrate that PRMT3-mediated YBX1-R69me2a modification promotes E2F1 oncogene expression by stabilizing NSUN2-catalysed m5C-modified E2F1 mRNA, thereby driving malignant progression of glioma. Aberrant activation of this axis is closely associated with higher tumor grade and unfavorable prognosis, highlighting PRMT3 and its catalysis of YBX1-R69 methylation as promising therapeutic targets and providing a strong rationale for the development of targeted therapies against this pathway.

DISCUSSION

GBM is characterized by marked molecular heterogeneity, aggressive growth, and inevitable recurrence [1]. Although major drivers such as aberrant EGFR signaling and IDH-defined molecular stratification have improved our understanding of GBM biology, the post-transcriptional circuits sustaining proliferative programs remain incompletely defined [24]. Here, we uncover a previously underappreciated oncogenic mechanism of PRMT3 in GBM. We demonstrate that PRMT3 catalyzes asymmetric dimethylation of YBX1 at Arg69, thereby enhancing YBX1 recognition and binding to m5C-modified transcripts. This modification selectively stabilizes m5C-marked E2F1 mRNA, leading to increased E2F1 protein expression and enhanced GBM cell proliferation (Fig. 10). Consistently, the coordinated association among PRMT3, YBX1-R69me2a, and E2F1 in clinical specimens, together with their

prognostic implications, supports PRMT3-YBX1-E2F1 as a key axis driving GBM progression and highlights its potential therapeutic relevance.

Protein arginine methyltransferases (PRMTs) have emerged as attractive promising therapeutic targets in cancer treatment [6, 25]. These enzymes regulate a diverse array of biological processes, including gene transcription, RNA splicing, post-translational modification (PTM), and DNA damage repair [13, 26]. PRMT3 is a member of the PRMT family broadly expressed in human tissues and harbors an N-terminal C2H2 zinc-finger motif implicated in substrate recognition [10]. Early studies established ribosomal protein S2(rpS2) as a canonical PRMT3 substrate and suggesting that rpS2 methylation by PRMT3 contributes to proper 80S ribosome maturation, positioning PRMT3 as a cytoplasmic arginine methyltransferase involved in translation and ribosome biogenesis [27, 28]. Recently, aberrant PRMT3 expression has been reported across multiple cancer types, including pancreatic cancer, colorectal cancer, and hepatocellular carcinoma, where elevated PRMT3 levels correlate with unfavorable clinical outcomes [10]. Mechanistically, PRMT3 has been shown to methylate and activate key metabolic enzymes (e.g., GAPDH-R248 and LDHA-R112), promote glycolytic reprogramming [29, 30], and amplify anabolic dependencies through stabilization of oncogenic proteins such as MYC [31]. Moreover, PRMT3-mediated methylation of hnRNPA1, METTL14, and IGF2BP1 has been implicated in chemotherapy resistance and stress adaptation [13, 14, 32]. Collectively, these studies underscore a context-dependent landscape of PRMT3 substrates and phenotypic outputs, supporting the notion that PRMT3 can function as a methylation hub coupling metabolism, immunity, and RNA regulatory programs [33].

In GBM, prior work has linked PRMT3 overexpression to poor prognosis and suggested a role in metabolic reprogramming, for instance via stabilizing HIF1A and promoting glycolysis to support tumor growth [16]. Extending these observations, we unexpectedly found that PRMT3 depletion attenuated EGFR phosphorylation without markedly altering total EGFR abundance, suggesting that PRMT3 may engage additional signaling modules to sustain oncogenic networks in GBM. To delineate the downstream mechanisms of PRMT3 in GBM, we performed Co-IP/MS and identified YBX1 as a candidate PRMT3-interacting protein. YBX1 is a well-established oncogenic and stress-adaptive DNA/RNA-binding protein whose functions are extensively shaped by posttranslational modifications, including phosphorylation, ubiquitination, acetylation, and glycosylation, which collectively influence its subcellular localization and regulatory outputs [19]. While phosphorylation of YBX1 at Ser102 has been implicated in nuclear translocation and transcription-associated functions [34, 35], we did not observe an appreciable change in p-YBX1(Ser102) upon PRMT3 perturbation, suggesting that PRMT3 regulates YBX1 through a distinct PTM-dependent mechanism. Consistently, multiple PTMs have been reported to control YBX1 nuclear-cytoplasmic shuttling and its transcript-regulatory functions across cancer contexts. Arginine methylation of YBX1 has only recently emerged as an important regulatory layer. Notably, PRMT5-dependent methylation of YBX1 has been linked to inflammatory signaling [36], and PRMT3-mediated methylation at other residues has been reported to modulate YBX1 phase-separation behavior in colorectal cancer [37]. In contrast, our work unveils a distinct and crucial methylation event: YBX1-R69me2a catalyzed by PRMT3. Importantly, we demonstrate that R69me2a substantially enhances

the RNA binding affinity of YBX1. This finding functionally links a “single-site PTM alteration” to a measurable “change in transcript half-life,” establishing a coherent causative cascade: PRMT3 enzymatic activity induces YBX1-R69me2a, thereby enhancing YBX1 RNA binding and stabilizing downstream transcripts. This clear mechanistic axis not only enhances biological plausibility but also reveals multiple druggable nodes for future therapeutic intervention, Importantly, our peptide competition experiments showed that a non-methylatable peptide could effectively compete with endogenous YBX1, reduce R69me2a levels, and suppress tumor growth to an extent comparable to YBX1-KO or YBX1-R69K. This compelling evidence suggests that the “methylation status” of this specific residue may itself be a viable therapeutic target.

To define a shared downstream effector of PRMT3 and YBX1, we integrated RNA-seq, eCLIP, and GO analyses, leading to the identification of E2F1. RIP-qPCR, actinomycin D chase experiments, and functional rescue support a model in which the PRMT3-YBX1 axis prolongs the half-life of m5C-modified E2F1 mRNA, leading to E2F1 protein accumulation and consequent upregulation of genes involved in cell cycle progression and DNA replication. While previous studies often emphasize deregulation of the Rb-E2F pathway or E2F1 gene amplification [38, 39], our findings reveal a posttranscriptional vulnerability whereby E2F1 output can be amplified through stabilization of an m5C-marked transcript. The concordance between PRMT3 overexpression, elevated E2F1 levels, and adverse clinical outcomes further supports the clinical relevance of this axis.

m5C-dependent regulation of transcript fate typically relies on the coordinated actions of methyltransferases ("writers"), binding proteins ("readers"), and demethylases ("erasers") [17, 40]. NSUN2 is a major mRNA m5C writer that modifies multiple RNA species and thereby influences RNA stability, processing, nuclear export, and translation [41, 42]. Accumulating evidence indicates that NSUN2 contributes to tumorigenesis by promoting proliferation, therapy resistance, epithelial-mesenchymal transition, and metabolic reprogramming [43]. However, our Co-IP/MS analysis did not support direct physical interaction between PRMT3 and NSUN2. Furthermore, neither our transcriptomic nor proteomic analyses revealed significant co-expression or regulatory relationships between them. This suggests that PRMT3 may not directly regulate NSUN2 in our experimental context. Intriguingly, we found a positive correlation between NSUN2 and the transcription factor E2F1. Recent studies, for instance in ovarian cancer, have established that NSUN2, in concert with the reader protein YBX1, regulates E2F1 expression through m5C-mediated stabilization of its mRNA [44]. Interestingly, our data suggests that PRMT3 can enhance YBX1's reader function. Thus, while PRMT3 does not appear to be part of the specific NSUN2-YBX1-E2F1 axis, it may potentially affect YBX1's general activity as an m5C reader. It is therefore plausible that PRMT3, by potentiating YBX1, contributes to the selective stabilization of oncogenic transcripts, thereby conferring a proliferative advantage through a mechanism parallel to, or integrated with, the NSUN2-YBX1 axis.

From a translational medicine perspective, our study delineates a dual therapeutic strategy. First, the small-molecule inhibitor SGC707 effectively suppresses PRMT3 enzymatic activity and demonstrates significant anti-tumor efficacy, thereby validating PRMT3 as a viable pharmacological target. Second, our

developed non-methylated peptide successfully inhibits tumor growth *in vivo* and *in vitro*. This suggests that directly targeting the YBX1-R69me2a interface may represent a more precise strategy than pan-PRMT3 inhibition, potentially mitigating off-target effects associated with disrupting broader PRMT3 functions. Intriguingly, we observed decreased EGFR phosphorylation upon PRMT3 knockdown despite unchanged total EGFR protein levels. Given that EGFR signaling is a core driver in GBM, this implies that PRMT3 may orchestrate a more complex oncogenic network beyond E2F1, possibly through phosphatase regulation or signaling crosstalk, which warrants further exploration.

In summary, our study demonstrates that PRMT3 promotes GBM cell proliferation by catalyzing YBX1-R69me2a, which enhances the YBX1-dependent stabilization of m5C-modified E2F1 mRNA and elevates E2F1 protein expression. This work tightly couples protein arginine methylation with epitranscriptomic regulation, providing a novel molecular logic for understanding GBM malignant progression and laying the groundwork for developing novel therapies targeting PRMT3 or disrupting the YBX1-RNA interaction.

MATERIALS AND METHODS

Clinical specimens

The study was approved by the Ethics Committee of The First Affiliated Hospital of USTC, Division of Life Sciences and Medicine. This investigation utilized 45 clinical tissue specimens, comprising 39 human glioma samples and 6 non-neoplastic brain tissues. The glioma cohort included 13 low-grade (WHO grade 2), 13 high-grade (WHO grade 3), and 13 GBM cases. All tissue samples were collected from patients diagnosed with glioma and post-surgical tumor resection. Written informed consent was obtained from all participants prior to tissue collection.

Cell lines and cell culture

Two human GBM cell lines (U87 and T98) and HEK293T cells, which obtained from the Cell Bank of the Chinese Academy of Sciences (Shanghai, China), were used in this study. Cells were propagated in Dulbecco's Modified Eagle Medium (DMEM; Gibco, MD, USA) enriched with 10% fetal bovine serum (FBS; Gibco) and incubated at 37°C in a humidified environment containing 5% CO_2.

Plasmids, shRNAs, siRNAs and sgRNA

The pcDNA3.1-PRMT3-FLAG^{WT}, pcDNA3.1-PRMT3-FLAG^{E338Q}, pcDNA3.1-YBX1-HA^{WT}, pcDNA3.1-YBX1-HA^{R69K}, pcDNA3.1-YBX1-HA^{R101K}, pcDNA3.1-E2F1-HA, and pcDNA3.1-NSUN2-HA plasmids were constructed by YouBio Biotechnology (Changsha, China). shRNA plasmids targeting PRMT3, PRMT3-specific siRNA, sgRNA plasmids targeting YBX1, YBX1-specific siRNA, E2F1-specific siRNA, and NSUN2-specific siRNA were synthesized by GenePharma (Suzhou, China). The validated sequences for shRNA, siRNA, and sgRNA are provided in Supplementary Table 1. Transfection procedures were performed by Lipofectamine 3000 reagent (Invitrogen, USA) in accordance with the manufacturer's protocol.

Lentivirus packaging and generation of stable cells

Gene-specific shRNA constructs targeting candidate genes were obtained from GenePharma (Suzhou, China) and validated by western blotting analysis. HEK293T cells were co-transfected with shRNA or sgRNA plasmid, PxpAx2 packaging plasmid, and PMD2g envelope plasmid (4:3:1) by Lipofectamine 3000 reagent. Viral supernatants were collected 48 hours post-transfection and filtered through 0.45 μm nitrocellulose membranes. GBM cells were then transduced with the filtered viral particles for 48 hours, followed by selection with 5 μg/mL puromycin for 1–2 weeks to establish stably transduced cell populations.

Quantitative Real-Time PCR (RT-qPCR)

Total RNA was extracted from cells by RNAiso Plus reagent, and complementary DNA (cDNA) was synthesized by reverse transcription following the manufacturer's protocol of the TOYOBO reverse transcription kit. Quantitative PCR reactions were prepared by Takara TB Green Premix Ex Taq II and performed on a Roche LightCycler system. The amplification protocol was carried out according to the manufacturer's recommended cycling conditions. Relative expression levels of target genes were calculated by the $2^{-\Delta\Delta Ct}$ method, with β-actin serving as the internal reference gene for normalization. All primers were synthesized by BGI Genomics, and the primer sequences are shown in Supplementary Table 2.

Western blotting

Cells or tissues were lysed in RIPA buffer supplemented with protease inhibitors at 4°C for 30 minutes, followed by homogenization via ultrasonication for 20 seconds. The lysates were centrifuged at 12,000×g for 10 minutes at 4°C, and the supernatant was collected for total protein quantification by a BCA assay kit. Proteins were denatured with 5×loading buffer by heating at 100°C for 10 minutes, and equal amounts (30 μg) of total protein were separated by 10%-12% SDS-polyacrylamide gel electrophoresis. Subsequently, proteins were transferred onto a nitrocellulose membrane (Millipore, MA, USA) under ice-cold conditions at a constant current of 300 mA. The membrane was blocked with 5% non-fat milk in TBST for 1 hour at room temperature with gentle shaking, followed by washing with TBST and incubation with primary antibodies at 4°C overnight with agitation. After further washing, the membrane was probed with species-appropriate horseradish peroxidase (HRP)-conjugated secondary antibodies for 1 hour at room temperature. Immunoreactive bands were visualized using an enhanced chemiluminescence (ECL) detection system, prepared by mixing reagent A and B at a 1:1 volume ratio, and exposed using a chemiluminescence imaging system. Relative protein levels were quantified using ImageJ software.

Hematoxylin and Eosin (H&E) staining

Tissue sections of 5 μm thickness containing the needle tract region were selected and baked at 60°C for 30–45 minutes. Deparaffinization and rehydration were performed through sequential immersion in xylene and a graded ethanol series. Sections were stained in hematoxylin solution for 5–10 minutes,

rinsed with distilled water for 2 minutes, and differentiated in 1% acid-alcohol for 5–20 seconds. After additional distilled water rinses, nuclear staining was verified microscopically, showing appropriate blue coloration with colorless cytoplasm. Sections were then washed under running tap water for 10 minutes and counterstained in eosin solution for approximately 5 minutes. Excess eosin was removed by gentle rinsing, and cytoplasmic pinkish-red staining was confirmed microscopically. Dehydration and clearing were achieved through a reverse graded ethanol series and xylene. Finally, sections were air-dried, mounted with 30 μL neutral balsam under coverslips, and imaged using light microscopy.

Immunohistochemistry (IHC)

Paraffin-embedded sections of human glioma or mouse brain tissues were prepared following standard fixation and dehydration protocols. Tissue sections of 5 μm thickness were mounted on poly-lysine-coated slides and subsequently processed for immunohistochemical analysis. The slides were first baked at 60°C for 40 minutes, followed by deparaffinization in xylene and rehydration through a graded ethanol series. Antigen retrieval was performed by pressure cooking in citrate buffer with two cycles of 3-minute boiling, with a cooling interval between cycles. After blocking with 10% normal goat serum for 1 hour at room temperature, the sections were incubated with appropriately diluted primary antibodies overnight at 4°C in a humidified chamber. Following three 5-minute PBS washes, the sections were incubated with corresponding secondary antibodies for 30 minutes at 37°C. After additional PBS washes, the sections were treated with Streptavidin-Biotin Complex (SABC) for 30 minutes at room temperature and then developed with DAB substrate for 1–3 minutes under microscopic monitoring. The reaction was stopped by distilled water rinsing. Counterstaining was performed with hematoxylin for 2 minutes, followed by differentiation in 1% acid alcohol and bluing under running tap water. Finally, the sections were dehydrated through a graded ethanol series, cleared in xylene, and mounted with neutral balsam. Images were acquired under a microscope, and quantitative analysis of positive signals was performed using ImageJ software.

Cell viability and proliferation assays

For cell viability assessment, stably transfected U87 and T98 cells (2×10^3 cells per well) were seeded in 96-well plates and cultured for 0–4 days. The cellular metabolic activity was examined after incubation with CCK-8 reagent (final concentration 10%) in a 37°C dark chamber for 1 hour. Absorbance measurements were obtained at 450 nm using a multifunctional microplate reader (Berthold Technology, USA). Colony formation capacity was evaluated by plating 1×10^3 cells per well in 6-well plates with 10-day culture. Following the incubation period, cells were immobilized in 4% paraformaldehyde and subjected to staining with 0.1% crystal violet solution. The stained colonies were documented photographically and enumerated using ImageJ software.

Immunofluorescence staining

U87 and T98 cells grown on sterile 35 mm coverslips were fixed with 4% paraformaldehyde at room temperature and permeabilized with 0.5% Triton X-100 for 10 minutes. Non-specific binding sites were blocked by incubation with 10% bovine serum albumin (BSA) for 1 hour at room temperature. Cells were

then incubated overnight at 4°C in a humidified chamber with primary antibodies against PRMT3 (Abcam, ab191562, 1:50) and YBX1 (santa cruz, sc-398340, 1:100). After three washes with PBS containing 0.1% Tween-20 (PBS-T), cells were incubated with fluorochrome-conjugated secondary antibodies for 1 hour at room temperature protected from light. Following three additional PBST washes, nuclei were counterstained with DAPI. The fluorescence images were acquired using a confocal fluorescence microscope.

Protein Co-immunoprecipitation assay

For endogenous co-immunoprecipitation, U87 and LN229 cells were lysed in NP-40 lysis buffer. Total protein lysates were collected, and 10% of the lysate was reserved as the input control. The remaining supernatant was pre-cleared by incubation with 30 μL of TBS-balanced Protein A/G magnetic beads for 1 hour at 4°C with rotation. The pre-cleared lysates were then incubated overnight at 4°C with rotation using anti-PRMT3 antibody, anti-YBX1 antibody, or control IgG. Immune complexes were captured by adding TBS-balanced Protein A/G magnetic beads and incubating for 2 hours at 4°C with rotation. Precipitated proteins were subsequently analyzed by immunoblotting using anti-PRMT3, anti-YBX1, anti-YBX1(R69me2a), or anti-aDMA antibody. For exogenous Co-immunoprecipitation, GBM cells or HEK293T cells were transfected with target plasmids, and lysates were prepared following the same procedure. After reserving 10% of the lysate as input, the remaining supernatant was incubated overnight at 4°C with rotation using anti-FLAG or anti-HA magnetic beads. Immunoprecipitated complexes were analyzed by immunoblotting with anti-FLAG, anti-HA, anti-YBX1(R69me2a), or anti-aDMA antibody.

RNA stability assay

Actinomycin D (MCE, 5μg/ ml) were added to treat targetting cells for 0, 2, 4, 8 hours. Then, cells were harvested for total RNA extraction. RT-qPCR was performed to measure the remaining E2F1 mRNA expression. β-actin was used as a reference.

RNA immunoprecipitation assay

We performed RNA immunoprecipitation (RIP) assay using Magna RIP™ Kit (Millipore) according to the manufacturer's instructions. Briefly, cells were lysed in a lysis buffer containing protease inhibitors and RNase inhibitors, followed by overnight rotation incubation at 4°C with protein A/G magnetic beads coated with YBX1 antibody. After immunoprecipitation, the beads were co-incubated with proteinase K to digest proteins, and RNA was subsequently purified using the phenol-chloroform method. Finally, RT-qPCR was performed to determine the enrichment of target RNA.

Liquid Chromatography-Tandem Mass Spectrometry (LC-MS/MS) analysis

Proteins were extracted from U87, T98, and PRMT3-overexpressing HEK293T cells using NP40 cell lysis buffer supplemented with protease inhibitors. Then, the protein lysates were pre-cleared with magnetic

beads. After incubating the cell lysates with PRMT3 antibody at 4°C overnight, magnetic beads were added for further incubation. The magnetic bead-PRMT3 antibody-protein complexes were sent to Hangzhou Cosmos Wisdom Biotech Co., Ltd. for LC/MS analysis of the proteins.

TAT-tagged peptide synthesis

The synthetic peptide sequence (KWFNVRNGYGFINR) corresponds to amino acids 64–77 of the YBX1 protein, containing the R69 methylation site, with a cell-penetrating TAT peptide conjugated to its N-terminal region to enhance cellular uptake. In the methylated peptide, the R69 site is di-methylated, whereas in the non-methylated peptide, the R69 site remains unmodified. For biotin conjugation, the biotin molecule was attached to the N-terminal region of the TAT peptide. All peptides were synthesized by GL Biochem (Shanghai) Ltd., purified by HPLC to > 95% purity, and verified by LC/MS.

Animal experiments

Animal procedures and experimental protocols were approved by the Animal Ethics Committee of The First Affiliated Hospital of USTC, Division of Life Sciences and Medicine. For intracranial orthotopic xenograft tumor assay, four-week-old female BALB/c-nu nude mice were anesthetized by intraperitoneal injection of sodium pentobarbital (40 mg/kg). After confirming stable respiration and loss of pedal withdrawal reflex, the animals were immobilized in a stereotactic frame. A cranial injection site was determined at a position 0.5 mm posterior to the bregma and 2.5 mm lateral to the midline. A small burr hole (0.8-1.0 mm in diameter) was drilled at the marked location using a micro-drill, with care taken to avoid meningeal or vascular injury. U87 cells transduced with either control shGFP or shPRMT3 lentiviral vectors were collected, resuspended, and intracranially injected through the burr hole using a micro-syringe at a depth of 2.5 mm below the dura mater. The injection was performed at a rate of 2 μL/min with a total volume of 10 μL. Postoperative body weight was monitored regularly. Significant weight loss or neurological deficits, indicative of impaired welfare due to intracranial tumor progression, were considered humane endpoints. At this stage, survival time was recorded, and mice were deeply anesthetized for transcardial perfusion followed by brain extraction. The harvested brain tissues were fixed in 4% paraformaldehyde and processed through graded ethanol dehydration, paraffin embedding, and sectioning for subsequent analysis. To measure the size of the tumor, the largest cross-section area of the tumor was selected. The formula for calculating the tumor volume is $V= (a \times b^2) / 2$, where a is the longest diameter and b is the shortest diameter. a and b are measured with Image J.

For subcutaneous xenograft tumor assay, U87 cells in optimal growth condition (1×10^7 cells) were suspended in 100 μL mixture of PBS and Matrigel (1:1), then subcutaneously injected into female BALB/c nude mice. Starting from day 5 post-implantation, the peptide solution (10 mg/kg) was administered via intraperitoneal injection every other day for a total of 2 weeks. Tumor size was measured using a vernier caliper along two perpendicular diameters, and tumor volume (mm^3) was calculated using the formula: $1/2 \times \text{length} \times \text{width}^2$. Tumor measurements were performed every 2 days beginning from day 5 of tumor growth. In this study, mice were observed daily until euthanasia at week 3. All subcutaneous tumor tissue samples were photographed and subsequently used for IHC analysis.

Bioinformatics analysis

In this study, we analyzed the expression of PRMT3 in pan-cancer using data from the TCGA database. The expression level of PRMT3 in glioma patients from the Rembrandt database and its impact on patient survival prognosis were examined by the GlioVis website (https://gliovis.bioinfo.cnio.es/). The classification of cell populations in glioma and the single-cell expression profile of PRMT3 across different cell clusters were analyzed using data from the TISCH website (https://tisch.compbio.cn/home/). Transcriptomic data following the knockdown of PRMT3 or YBX1 in GBM cells were evaluated using Dataset GSE200902 and GSE213046. eCLIP-seq data was utilized to identify potential RNA molecules interacting with the YBX1 protein in GBM cells [22].

Statistical analysis

All statistical analyses were performed using SPSS 22.0 (Chicago, USA) and GraphPad Prism 8.0. Data are presented as mean ± standard deviation (SD) from at least three independent experiments. Comparison between two groups was performed using two-tailed Student's t-test or Wilcoxon rank-sum test, while multiple group comparisons were conducted using one-way analysis of variance (ANOVA) followed by Dunnett's or Tukey's multiple comparison tests. Survival analysis was performed using the Kaplan-Meier method with log-rank tests for between-curve comparisons. In all analyses, a p-value less than 0.05 was considered statistically significant.

Declarations

DATA AVAILABILITY

Data is provided within the manuscript or supplementary information files. The remaining data are available from the authors upon request.

ACKNOWLEDGEMENTS

The authors are grateful for the convenience provided by all public databases used in this study (TCGA, CGGA, GEO, TISCH2 and Rembrandt). This work was supported by grants from National Natural Science Foundation of China (82303851, Ji Wang), Guangdong Basic and Applied Basic Research Foundation (2022A1515111065), and the China Postdoctoral Science Foundation (2023M740840).

COMPETING INTERESTS

The authors declare no conflict of interest.

AUTHOR CONTRIBUTIONS

Fei Wang, Nan Peng, Haibo Wu, Xuanzhi Wang, and Ji Wang designed and supervised the study. Ji Wang, Shiquan Shen, Dongshan Zhang, and Honglong Zhou performed the experiments. Zongyu Xiao, Tianran Chai, Xinzhi Wu, Minghui Zeng, Li Jia, Zheng Li, Songsong Lu, and Yang Tu collected the data and performed statistical analyses. Zheng Li, Songsong Lu, and Yang Tu provided clinical samples. Ji Wang,

Shiquan Shen, and Fei Wang wrote the manuscript. Fei Wang, Nan Peng, Haibo Wu, Xuanzhi Wang, and Ji Wang finally reviewed the manuscript. All authors have approved the final manuscript.

References

1. Tang J, Karbhari N, Campian JL. Therapeutic targets in glioblastoma: molecular pathways, emerging strategies, and future directions. Cells. 2025;14:494.
2. Louis DN, Perry A, Wesseling P, Brat DJ, Cree IA, Figarella-Branger D, et al. The 2021 WHO classification of tumors of the central nervous system: a summary. Neuro Oncol. 2021;23:1231–1251.
3. Królikowska K, Błaszczak K, Ławicki S, Zajkowska M, Gudowska-Sawczuk M. Glioblastoma-a contemporary overview of epidemiology, classification, pathogenesis, diagnosis, and treatment: a review article. Int J Mol Sci. 2025;26:12162.
4. Isachesku E, Braicu C, Pirlog R, Kocijancic A, Busuioc C, Pruteanu LL, et al. The role of non-coding RNAs in epigenetic dysregulation in glioblastoma development. Int J Mol Sci. 2023;24:16320.
5. Stitzlein LM, Adams JT, Stitzlein EN, Dudley RW, Chandra J. Current and future therapeutic strategies for high-grade gliomas leveraging the interplay between epigenetic regulators and kinase signaling networks. J Exp Clin Cancer Res. 2024;43:12.
6. Shen S, Zhou H, Xiao Z, Zhan S, Tuo Y, Chen D, et al. PRMT1 in human neoplasm: cancer biology and potential therapeutic target. Cell Commun Signal. 2024;22:102.
7. Wang X, Zhu B, Winn R, Lu S, Wang H. Functional dynamics of arginine mono- and di-methylation. Cells. 2025;14:796.
8. Xu Y, Wu Q, Zhang Y, Gu Y, Zhu H, Fu X, et al. Arginine methylation in cancer: mechanisms and therapeutic implications. Biomark Res. 2025;13:143.
9. Hang R, Liu C, Ahmad A, Zhang Y, Lu F, Cao X. Arabidopsis protein arginine methyltransferase 3 is required for ribosome biogenesis by affecting precursor ribosomal RNA processing. Proc Natl Acad Sci USA. 2014;111:16190–16195.
10. Hsu SH, Hung WC. Protein arginine methyltransferase 3: A crucial regulator in metabolic reprogramming and gene expression in cancers. Cancer Lett. 2023;554:216008.
11. Zhi R, Wu K, Zhang J, Liu H, Niu C, Li S, et al. PRMT3 regulates the progression of invasive micropapillary carcinoma of the breast. Cancer Sci. 2023;114:1912–1928.
12. Zhang S, Wang S, Wang Y, Zhou T, Yang J, Xu J, et al. PRMT3 drives IDO1-dependent radioresistance and immunosuppression by promoting kynurenine metabolism in non-small cell lung cancer. Cancer Res. 2026;86:421–437.
13. Shi Y, Niu Y, Yuan Y, Li K, Zhong C, Qiu Z, et al. PRMT3-mediated arginine methylation of IGF2BP1 promotes oxaliplatin resistance in liver cancer. Nat Commun. 2023;14:1932.
14. Wang Y, Wang C, Guan X, Ma Y, Zhang S, Li F, et al. PRMT3-mediated arginine methylation of METTL14 promotes malignant progression and treatment resistance in endometrial carcinoma. Adv

Sci (Weinh). 2023;10:e2303812.
15. Zhang X, Wang K, Feng X, Wang J, Chu Y, Jia C, et al. PRMT3 promotes tumorigenesis by methylating and stabilizing HIF1α in colorectal cancer. Cell Death Dis. 2021;12:1066.
16. Liao Y, Luo Z, Lin Y, Chen H, Chen T, Xu L, et al. PRMT3 drives glioblastoma progression by enhancing HIF1A and glycolytic metabolism. Cell Death Dis. 2022;13:943.
17. Zhang J, Che P, Yang Z, Zhang P, Shui Y, Lu X, et al. The m5C reader Ybx1 regulates embryonic cortical neurogenesis by promoting progenitor cell cycle progression. PLoS Biol. 2025;23:e3003175.
18. Dinh NTM, Nguyen TM, Park MK, Lee CH. Y-box binding protein 1: unraveling the multifaceted role in cancer development and therapeutic potential. Int J Mol Sci. 2024;25:717.
19. Zhang W, Liu Y, Zhao Z, Zhang Y, Liang Y, Wang W. YBX1: a multifunctional protein in senescence and immune regulation. Curr Issues Mol Biol. 2024;46:14058–14079.
20. Li X, Chen G, Liu B, Tao Z, Wu Y, Zhang K, et al. PLK1 inhibition promotes apoptosis and DNA damage in glioma stem cells by regulating the nuclear translocation of YBX1. Cell Death Discov. 2023;9:68.
21. Seres M, Spacayova K, Sulova Z, Spaldova J, Breier A, Pavlikova L. Dynamic multilevel regulation of EGFR, KRAS, and MYC oncogenes: driving cancer cell proliferation through (Epi)genetic and post-transcriptional/translational pathways. Cancers (Basel). 2025;17:248.
22. Zheng C, Wei Y, Zhang Q, Sun M, Wang Y, Hou J, et al. Multiomics analyses reveal *DARS1-AS1*/YBX1-controlled posttranscriptional circuits promoting glioblastoma tumorigenesis/radioresistance. Sci Adv. 2023;9:eadf3984.
23. Manickavinayaham S, Velez-Cruz R, Biswas AK, Chen J, Guo R, Johnson DG. The E2F1 transcription factor and RB tumor suppressor moonlight as DNA repair factors. Cell Cycle. 2020;19:2260–2269.
24. Xie Q, Wu TP, Gimple RC, Li Z, Prager BC, Wu Q, et al. N^6-methyladenine DNA modification in glioblastoma. Cell. 2018;175:1228–1243.e20.
25. Wang J, Xiao Z, Li P, Wu C, Li Y, Wang Q, et al. PRMT6-CDC20 facilitates glioblastoma progression via the degradation of CDKN1B. Oncogene. 2023;42:1088–1100.
26. Hwang JW, Cho Y, Bae GU, Kim SN, Kim YK. Protein arginine methyltransferases: promising targets for cancer therapy. Exp Mol Med. 2021;53:788–808.
27. Swiercz R, Person MD, Bedford MT. Ribosomal protein S2 is a substrate for mammalian PRMT3 (protein arginine methyltransferase 3). Biochem J. 2005;386:85–91.
28. Bachand F, Silver PA. PRMT3 is a ribosomal protein methyltransferase that affects the cellular levels of ribosomal subunits. EMBO J. 2004;23:2641–2650.
29. Lei Y, Han P, Chen Y, Wang H, Wang S, Wang M, et al. Protein arginine methyltransferase 3 promotes glycolysis and hepatocellular carcinoma growth by enhancing arginine methylation of lactate dehydrogenase A. Clin Transl Med. 2022;12:e686.
30. Hsu MC, Tsai YL, Lin CH, Pan MR, Shan YS, Cheng TY, et al. Protein arginine methyltransferase 3-induced metabolic reprogramming is a vulnerable target of pancreatic cancer. J Hematol Oncol.

2019;12:79.
31. Hu Y, Su Y, He Y, Liu W, Xiao B. Arginine methyltransferase PRMT3 promote tumorigenesis through regulating c-MYC stabilization in colorectal cancer. Gene. 2021;791:145718.
32. Hsu MC, Pan MR, Chu PY, Tsai YL, Tsai CH, Shan YS, et al. Protein arginine methyltransferase 3 enhances chemoresistance in pancreatic cancer by methylating hnRNPA1 to increase ABCG2 expression. Cancers (Basel). 2018;11:8.
33. Hou H, Meng J, Chen Y, Zhang X, Yang Z, Wang Q, et al. PRMT3 at the crossroads of inflammation: dual roles in metabolic reprogramming and immune dysregulation in chronic diseases. Front Immunol. 2026;16:1663258.
34. Alkrekshi A, Wang W, Rana PS, Markovic V, Sossey-Alaoui K. A comprehensive review of the functions of YB-1 in cancer stemness, metastasis and drug resistance. Cell Signal. 2021;85:110073.
35. Kuwano M, Shibata T, Watari K, Ono M. Oncogenic Y-box binding protein-1 as an effective therapeutic target in drug-resistant cancer. Cancer Sci. 2019;110:1536–1543.
36. Hartley AV, Wang B, Mundade R, Jiang G, Sun M, Wei H, et al. PRMT5-mediated methylation of YBX1 regulates NF-κB activity in colorectal cancer. Sci Rep. 2020;10:15934.
37. Shi Y, Wan T, Liu S, Liu H, Zeng Z, Li W, et al. Dynamic arginine methylation of YBX1 relay controls its phase separation and chemoradiotherapy resistance in rectal cancer. Adv Sci (Weinh). 2025;12:e02786.
38. Olmez I, Zhang Y, Manigat L, Benamar M, Brenneman B, Nakano I, et al. Combined c-Met/Trk inhibition overcomes resistance to CDK4/6 inhibitors in glioblastoma. Cancer Res. 2018;78:4360–4369.
39. Xu L, Chen Y, Mayakonda A, Koh L, Chong YK, Buckley DL, et al. Targetable BET proteins- and E2F1-dependent transcriptional program maintains the malignancy of glioblastoma. Proc Natl Acad Sci USA. 2018;115:E5086-E5095.
40. Guan Z, Li W, He Y, Guo W. RNA m5C methylation in cancer: mechanisms and biological impact. Oncogenesis. 2025;14:44.
41. Jiang T, Jiang N, Chen X, Xiong Z. The role of NSUN family genes in m5C methylation and diseases. Biomedicines. 2025;13:2951.
42. Li P, Huang D. NSUN2-mediated RNA methylation: molecular mechanisms and clinical relevance in cancer. Cell Signal. 2024;123:111375.
43. Li C, Yuan Y, Jiang X, Wang Q. Roles and mechanisms of NSUN2-mediated RNA m^5C modification in cancer progression and immune modulation. Front Immunol. 2025;16:1702436.
44. Liu X, Wei Q, Yang C, Zhao H, Xu J, Mobet Y, et al. RNA m^5C modification upregulates E2F1 expression in a manner dependent on YBX1 phase separation and promotes tumor progression in ovarian cancer. Exp Mol Med. 2024;56:600–615.

Figures

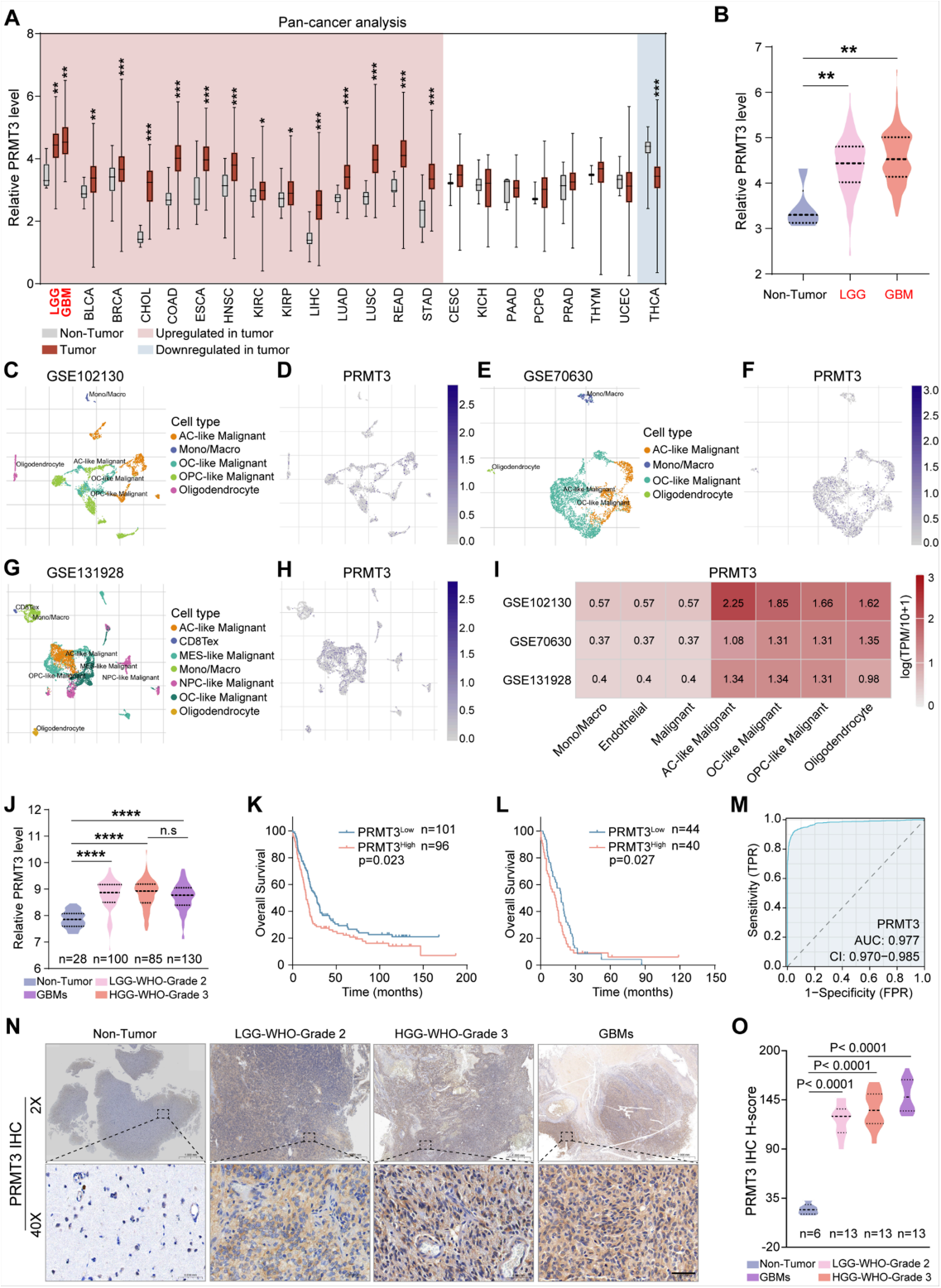


Figure 1

PRMT3 is overexpressed in glioma and correlates with poor prognosis. A Pan-cancer analysis of PRMT3 mRNA expression across tumor and corresponding normal tissues in the TCGA database. **B** Differential expression of PRMT3 between lower-grade glioma (LGG) or glioblastoma (GBM) and non-tumor brain tissues in the TCGA cohort. **C-I** PRMT3 expression across different cell types in single-cell RNA-sequencing datasets GSE102130 (**C**,**D**), GSE70630 (**E**, **F**) and GSE131928 (**G**, **H**), with

pooled results summarized in (**I**). **J** The expression profile of PRMT3 in non-tumor tissue, LGG (WHO grade 2), HGG (WHO grade 3) and GBM samples from the Rembrandt database. **K**, **L** Kaplan-Meier curves showing the association between high/low PRMT3 expression and overall survival (OS) in all glioma patients (**K**) and in GBM patients alone (**L**) in the Rembrandt cohort. **M** The receiver operating characteristic (ROC) curve for evaluating the diagnostic performance of PRMT3 in glioma based on PRMT3 expression data from glioma patients in the Rembrandt database. **N**Representative IHC images of PRMT3 protein expression in non-tumor brain tissue, LGG (WHO grade 2), HGG (WHO grade 3) and GBM samples. Scale bar, 50 μm. **O** Quantification of IHC staining intensity (H-score) in non-tumor tissues (n=6), LGG (n=13), HGG (n=13) and GBM (n=13). Data are presented as mean ± SD. **P* < 0.05, ***P* < 0.01, ****P* < 0.001, ****P*< 0.0001, n.s, not significant, versus the indicated groups, Student's t-test.

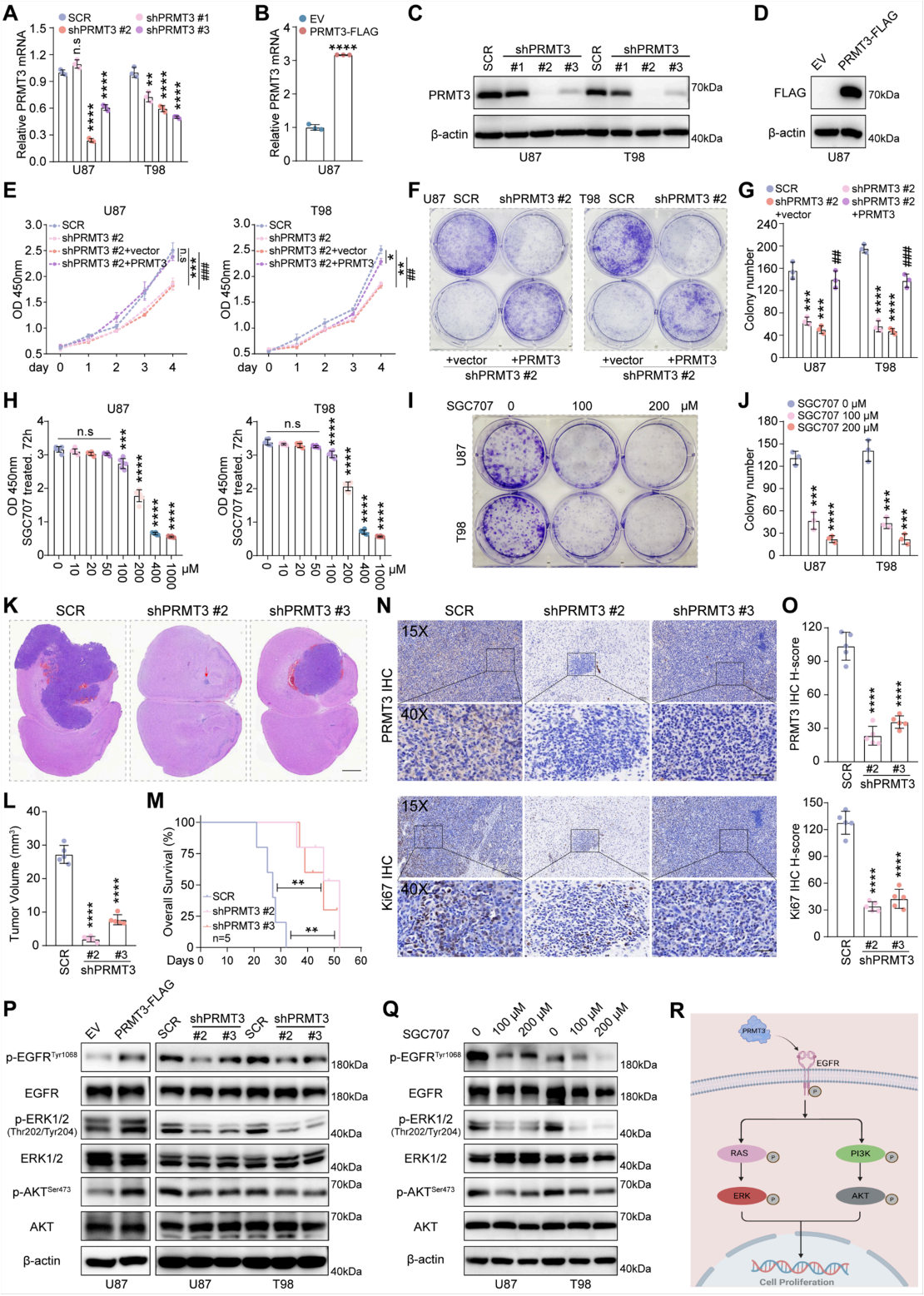


Figure 2

PRMT3 promotes GBM cell proliferation *in vitro* and *in vivo*. A, **B** The RT-qPCR results validating the knockdown efficiency of PRMT3 using three independent shRNA sequences (shPRMT3#1-3) in U87 and T98 cells (**A**), as well as the results verifying the overexpression efficiency of PRMT3 plasmid in U87 cells (**B**). **C**, **D** Western blotting analysis of PRMT3 protein levels in U87 and T98 cells transduced with shPRMT3 (**C**) or PRMT3 overexpression plasmids (**D**). β-actin was used as a loading control. **E** CCK-8

assay showing proliferation curves of U87 and T98 cells in the indicated groups (SCR, shPRMT3#2, shPRMT3+vector, and shPRMT3+PRMT3-OE). **F**, **G** Representative images (**F**) and quantification (**G**) of colony formation assays in U87 and T98 cells following PRMT3 knockdown and rescue experiments. **H** Dose-response curves of U87 and T98 cells treated with the PRMT3 inhibitor SGC707 at indicated concentrations for 72 hours, assessed by CCK-8 assay. **I**, **J** Representative images (**I**) and quantification (**J**) of colony formation in U87 and T98 cells treated with SGC707 (0, 100, 200 μM) for 10 days. **K-M** A mouse intracranial orthotopic xenograft model was established using U87 cells transfected with shPRMT3 (#2, #3) and SCR cells. Representative H&E staining of whole brain sections (**K**) and quantification of tumor area (**L**) in each group of mice. Kaplan-Meier survival curves of tumor-bearing mice (**M**) in each group of mice; *P* values were determined by log-rank test. Scale bar, 5 μm. **N**, **O** Representative IHC staining images of PRMT3 and Ki67 in xenograft tumor tissues from each group (**N**) and quantitative H-score values (**O**). Scale bar, 50 μm. **P** Western blotting analysis of EGFR/ERK/AKT signaling expression in PRMT3-overexpressing U87 cells (left) and PRMT3-knockdown U87/T98 cells (right). **Q** Immunoblotting analysis of EGFR/ERK/AKT pathway expression in U87 and T98 cells treated with SGC707 (0, 100, 200 μM). **R** Schematic diagram depicting the proposed mechanism by which PRMT3 activates the EGFR/AKT/ERK signaling axis in GBM cell. Data are presented as mean ± SD. *in vitro* assays, n = 3 independent experiments; *in vivo* studies, n = 5 mice per group. * vs. control group, **P* < 0.05, ***P* < 0.01, ****P* < 0.001, ****P* < 0.0001, $^{\#}$ vs. shPRMT3 #2 + vector group, $^{\#\#}P$ < 0.01, $^{\#\#\#}P$ < 0.001, n.s, not significant, versus the indicated groups, Student's t-test.

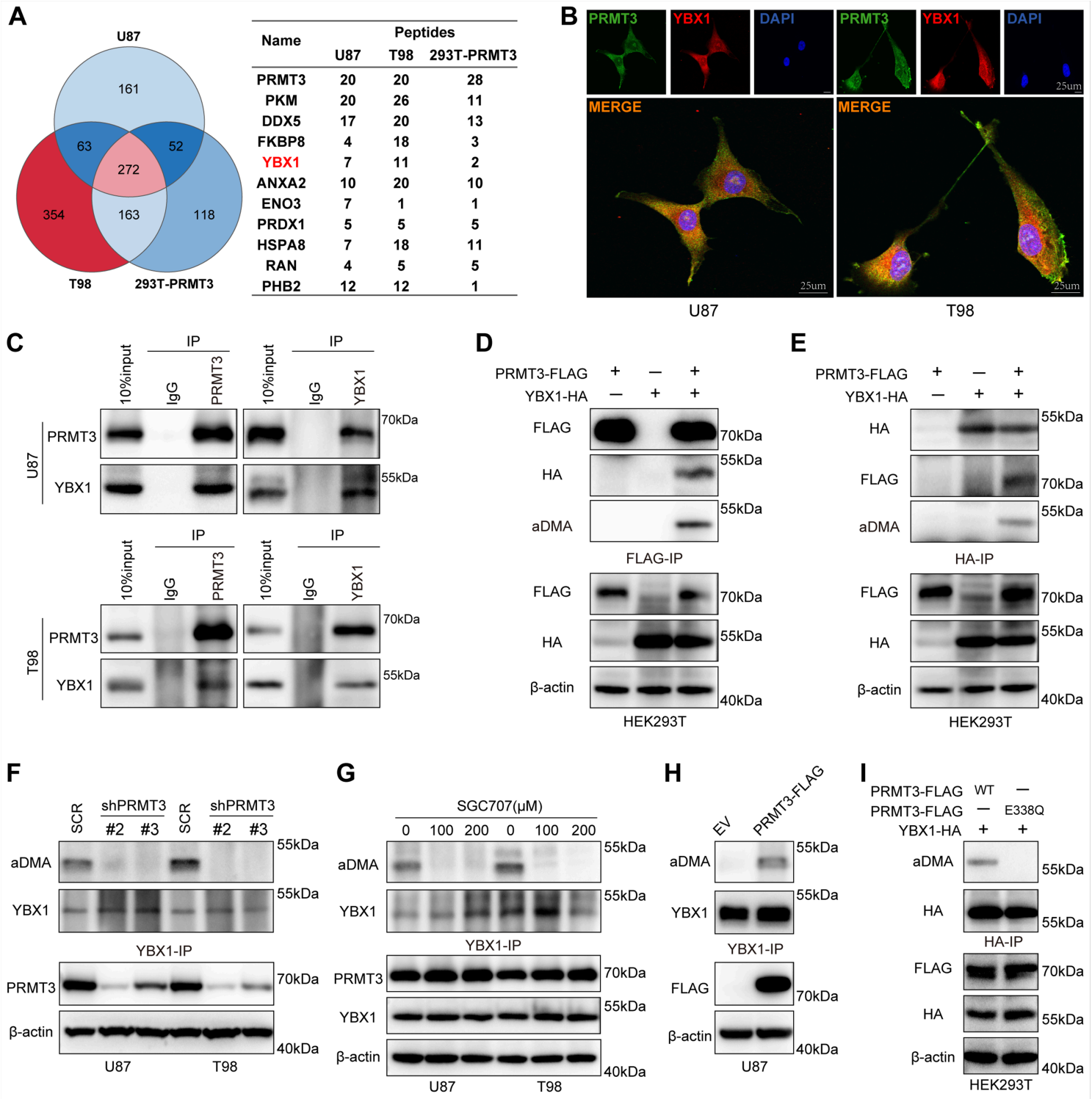


Figure 3

PRMT3 mediates arginine methylation of YBX1. A Venn diagram showing the overlap of PRMT3-interacting proteins identified by LC-MS/MS in U87, T98, and HEK293T cells. **B**Representative immunofluorescence images showing the colocalization of PRMT3 (green) and YBX1 (red) in the cytoplasm of U87 and T98 cells. Nuclei were stained with DAPI (blue). Scale bar, 25 μm. **C**Lysates from U87 and T98 cells were subjected to reciprocal Co-immunoprecipitation (IP) with anti-PRMT3 and anti-YBX1 antibodies, followed by immunoblotting (IB) with anti-YBX1 and anti-PRMT3 antibodies. IgG was

used as a negative control. **D**, **E** Interaction and methylation analysis of exogenous PRMT3 and YBX1. HEK293T cells were co-transfected with Flag-tagged PRMT3 and HA-tagged YBX1 expression plasmids. Co-IP assays were performed using anti-FLAG magnetic beads (**D**) or anti-HA magnetic beads for reciprocal IP (**E**). The physical interaction between PRMT3 and YBX1, as well as the levels of asymmetric dimethylarginine (aDMA), were analyzed by western blotting with the indicated antibodies. **F**, **G** U87 and T98 cells were transfected with shPRMT3 (**F**) or treated with the PRMT3 inhibitor SGC707 (**G**). Endogenous YBX1 was immunoprecipitated, and methylation levels were assessed using an anti-aDMA antibody. Total YBX1 in the Co-IP products served as the loading control. **H**U87 cells were transfected with PRMT3 or control vector, and aDMA levels on YBX1 were examined by anti-aDMA IB after YBX1 IP. **I**HEK293T cells were co-transfected with YBX1-HA and PRMT3-FLAG (WT) or PRMT3-FLAG (E338Q, catalytically inactive mutant) plasmids. Co-IP was performed with anti-HA beads, followed by immunoblotting for aDMA antibody.

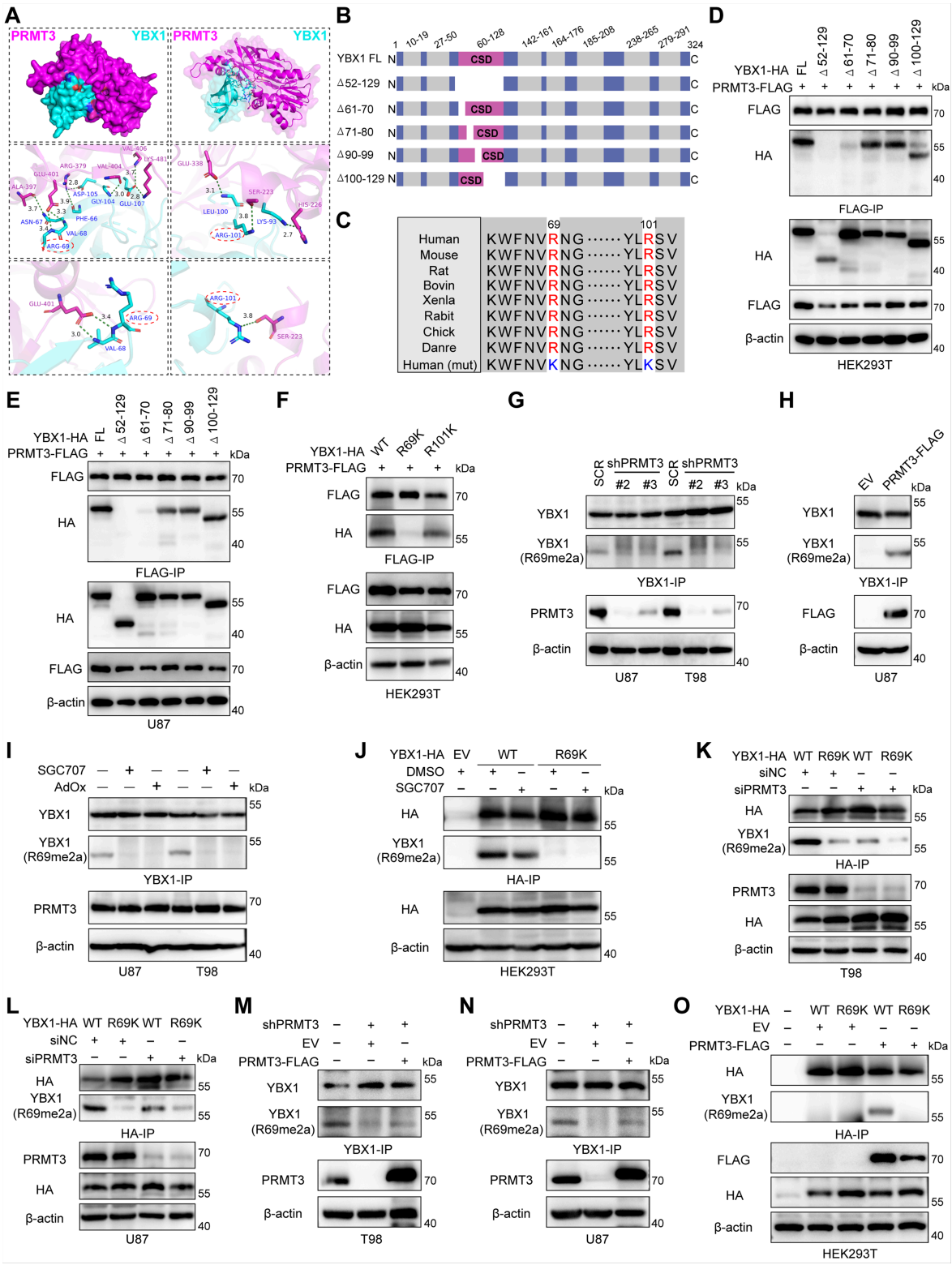


Figure 4

PRMT3 methylates YBX1 at R69 within its cold-shock domain. A Structural prediction of the PRMT3-YBX1 complex using AlphaFold3 reveals Arginine 69 (R69) and Arginine 101 (R101) within the YBX1 cold-shock domain (CSD) as potential methylation sites at the interaction interface. **B** Schematic diagram of YBX1 protein structural composition and CSD deletion mutants used for mapping PRMT3 binding regions. **C** The protein sequence alignment of the YBX1 CSD from the indicated species showing

high conservation of R69 and R101. Schematic of the arginine-to-lysine point mutants (R69K and R101K) generated for functional analysis. **D**, **E** Mapping of the PRMT3-binding region in YBX1 by Co-IP. HEK293T (**D**) and U87 (**E**) cells were co-transfected with PRMT3-FLAG and HA-tagged full-length or CSD-deletion mutants of YBX1 plasmids. PRMT3 complexes were isolated using anti-FLAG beads and analyzed by immunoblotting with an anti-HA antibody to detect associated YBX1 constructs. **F** HEK293T cells were co-transfected with PRMT3-FLAG and YBX1-HA WT, R69K, or R101K mutants' plasmids. Following immunoprecipitation of PRMT3 with anti-FLAG beads, co-precipitated YBX1 was detected by immunoblotting with an anti-HA antibody. **G-I** Endogenous YBX1 was immunoprecipitated from U87 and T98 cells upon PRMT3 knockdown (**G**), PRMT3 overexpression (**H**), or treatment with SGC707 or AdOx (methylation inhibitor, 100 μM) (**I**), and YBX1-R69 methylation levels were assessed by immunoblotting with the anti-YBX1-R69me2a antibody. **J** HA-tagged YBX1 (WT or R69K) plasmids were expressed in HEK293T cells and then treated or not with SGC707 (100 μM). Immunoprecipitation with anti-HA beads followed by immunoblotting with the anti-YBX1-R69me2a antibody was performed to determine YBX1-R69 methylation levels. **K**, **L** T98 (**K**) and U87 (**L**) cells were transfected with HA-tagged YBX1 (WT or R69K) plasmids and further infected with control or PRMT3-targeting siRNA. YBX1 was immunoprecipitated with anti-HA beads, and YBX1-R69 methylation levels were assessed by immunoblotting. **M**, **N** T98 (**M**) and U87 (**N**) cells with stable PRMT3 knockdown were reconstituted with exogenous PRMT3 or control vector. Endogenous YBX1 was immunoprecipitated with an anti-YBX1 antibody, and YBX1-R69 methylation levels were analyzed by immunoblotting. **O** HEK293T cells were transfected with YBX1-HA (WT or R69K) alone or co-transfected with PRMT3-FLAG plasmids. YBX1 methylation was detected via immunoprecipitated with anti-HA beads followed by western blotting with anti-YBX1-R69me2a antibody.

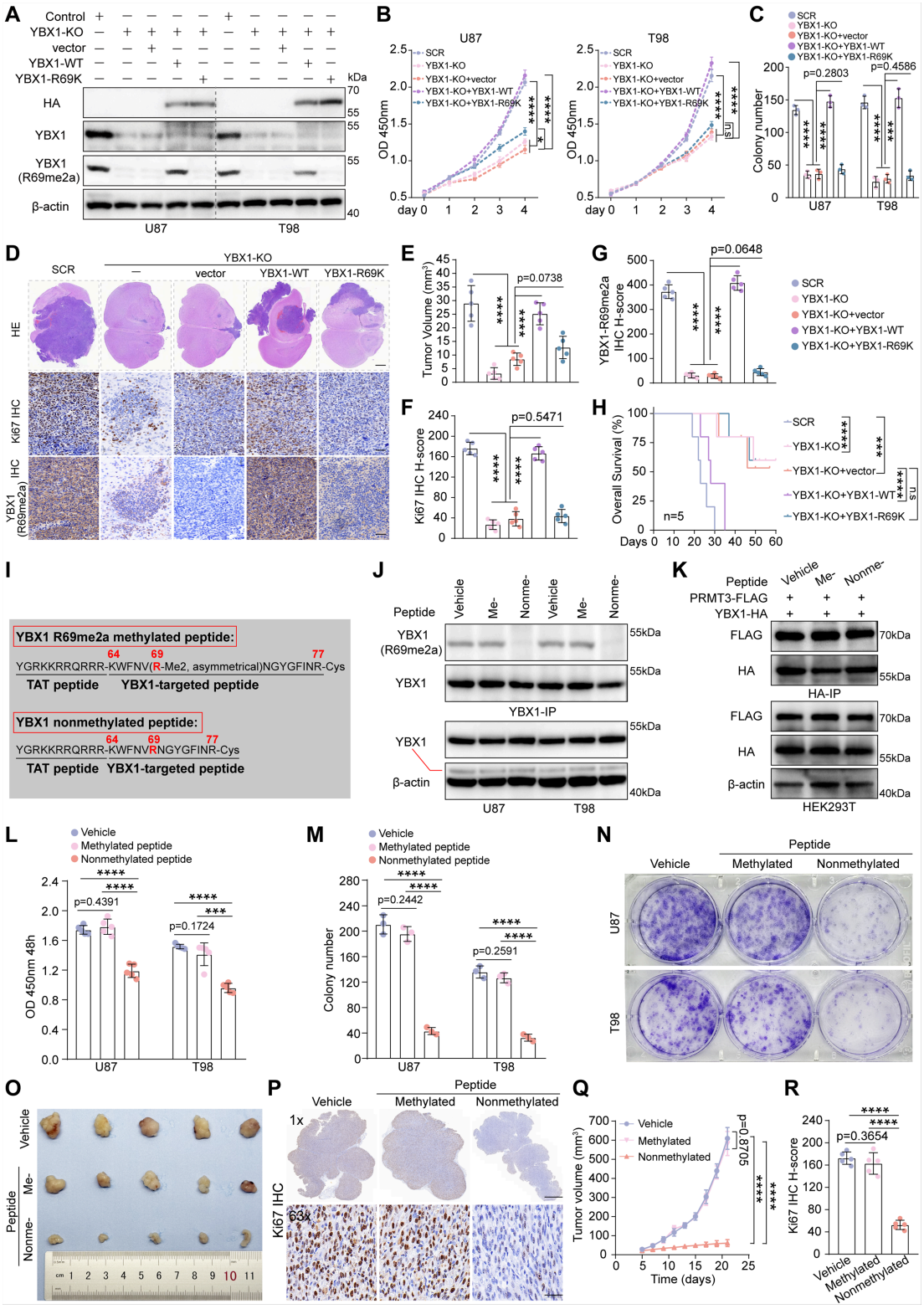


Figure 5

Targeting YBX1-R69 methylation suppresses GBM cell growth *in vitro* and *in vivo*. **A** YBX1-KO U87 and T98 cells were reconstituted with YBX1-WT or YBX1-R69K mutant lentiviruses. The level of YBX1-R69me2a was detected by western blotting, showing specific loss of methylation in the R69K mutant (total YBX1 was examined as a control). **B** U87 and T98 cells with YBX1 knockout (YBX1-KO) were reconstituted with vector control, YBX1-WT, or YBX1-R69K. Cell proliferation was assessed by CCK-8

assays at the indicated time points. **C** Quantification of colony formation in YBX1-KO cells reconstituted with vector control, YBX1-WT or YBX1-R69K. **D-H** Representative H&E and IHC staining for Ki67 and YBX1-R69me2a in brain sections from mice implanted intracranially with U87 YBX1-KO cells reconstituted with vector control, YBX1-WT or YBX1-R69K (**D**). Quantification of intracranial tumor size based on H&E staining (**E**). Scale bar, 5 μm. Quantification of Ki67 (**F**) and YBX1-R69me2a (**G**) IHC H-scores. Scale bar, 50 μm. Kaplan-Meier survival curves of mice bearing intracranial tumors derived from YBX1-WT- or YBX1-R69K-reconstituted U87 YBX1-KO cells (**H**). P values were determined by log-rank test. **I** Schematic representation of the amino acid sequences of the TAT-nonmethylated peptide and the TAT-methylated peptide. **J** U87 and T98 cells were treated with 20 μM peptides for 48 h. Lysates were immunoprecipitated with anti-YBX1 antibody, and YBX1-R69 methylation was analyzed by immunoblotting using a site-specific anti-YBX1 R69me2a antibody. **K** HEK293T cells co-transfected with PRMT3-FLAG and YBX1-HA plasmids, and then were treated with YBX1-methylated or YBX1-nonmethylate peptides (20 μM, 48 hours), followed by immunoprecipitated with anti-HA beads and western blotting analysis. **L** U87 and T98 cells were treated with YBX1-methylated or YBX1-nonmethylate peptides for 48 h, and analyzed for viability by CCK-8 assay. **M**, **N** U87 and T98 cells were seeded in 6-well plates and treated with YBX1-methylated or YBX1-nonmethylate peptides (20 μM) for 10 days. Colonies were fixed, stained, and quantified (**M**), with representative images shown in (**N**). **O-R** Nude mice bearing established subcutaneous U87 xenografts were randomized to receive peptides (10 mg/kg, intraperitoneally, every other day for 2 weeks). Images of tumors obtained at the observation endpoint (**O**). Representative IHC staining for Ki67 in tumor tissues (**P**). Scale bar, 10 μm. Tumor volume growth curves (**Q**). Quantification of Ki67 IHC staining (H-score) (**R**). Data are presented as mean ± SD. **P*< 0.05, ****P* < 0.001, ****P* < 0.0001, n.s, not significant, versus the indicated groups, Student's t-test.

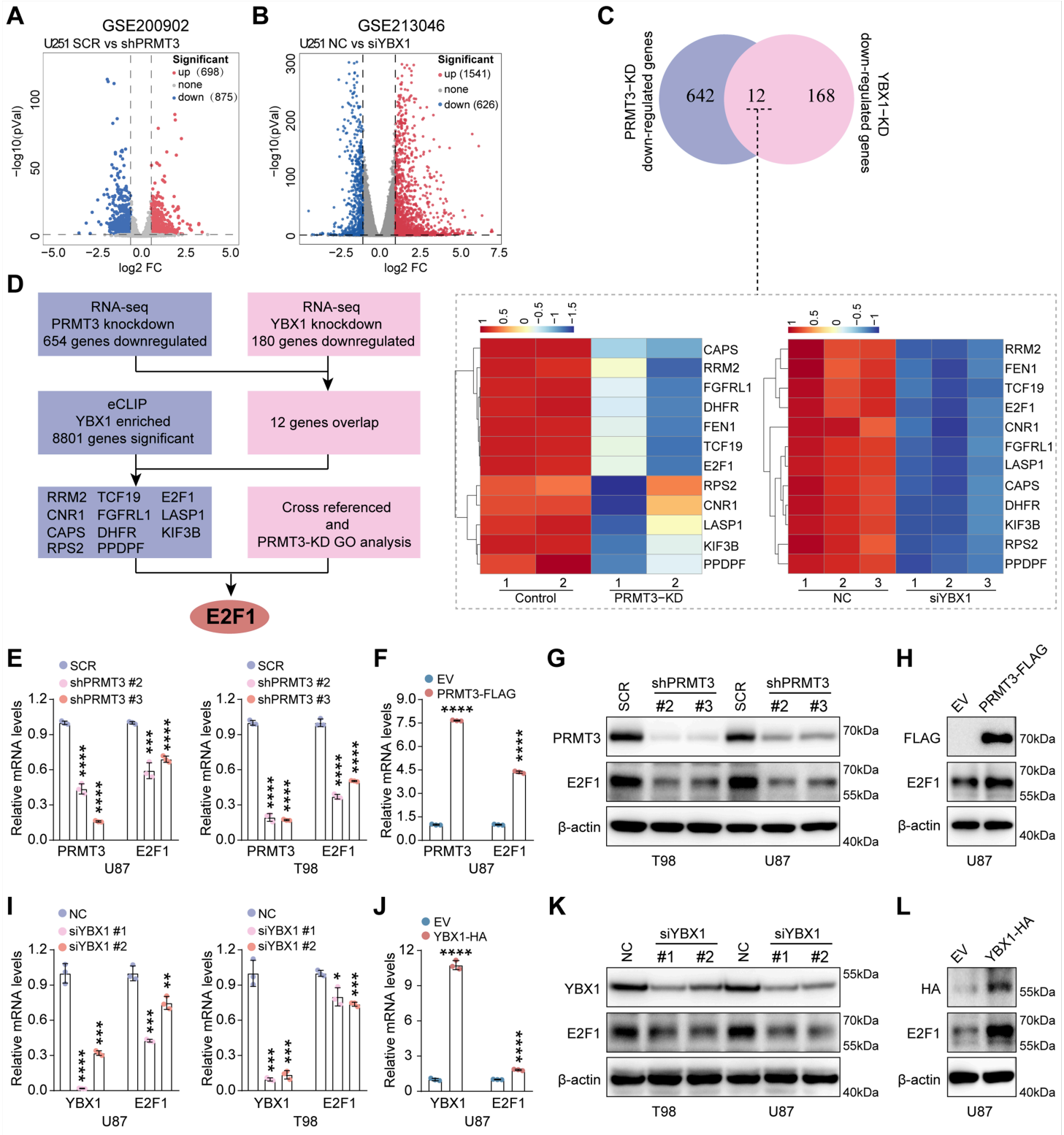


Figure 6

E2F1 is identified as a key downstream target of the PRMT3-YBX1 axis. A, **B** Volcano plots showing differentially expressed genes in the GSE20092 (**A**) and GSE213046 (**B**) datasets. **C** (Upper) Venn diagram showing the intersection of downregulated genes following either PRMT3 or YBX1 knockdown in U251 cells. (Lower) The heatmap depicts the expression profiles of the 12 overlapping genes. **D** Schematic workflow illustrating the integration of RNA-seq, eCLIP, and GO analyses to identify E2F1 as a

common downstream target of the PRMT3-YBX1 axis. **E**, **F** RT-qPCR analysis of E2F1 mRNA levels in U87 and T98 cells following PRMT3 knockdown (**E**), and in U87 cells upon PRMT3 overexpression (**F**). **G**, **H** Western blotting analysis of E2F1 protein levels in U87 and T98 cells following PRMT3 knockdown (**G**), and in U87 cells upon PRMT3 overexpression (**H**). **I**, **J** RT-qPCR analysis of E2F1 mRNA levels in U87 and T98 cells with YBX1 knockdown (**I**), and in U87 cells with YBX1 overexpression (**J**). **K**, **L** Immunoblotting analysis of E2F1 protein levels in U87 and T98 cells with YBX1 knockdown (**K**), and in U87 cells with YBX1 overexpression (**L**). Data are presented as mean ± SD. *P < 0.05, **P < 0.01, ***P< 0.001, ***P < 0.0001, versus the indicated groups, Student's t-test.

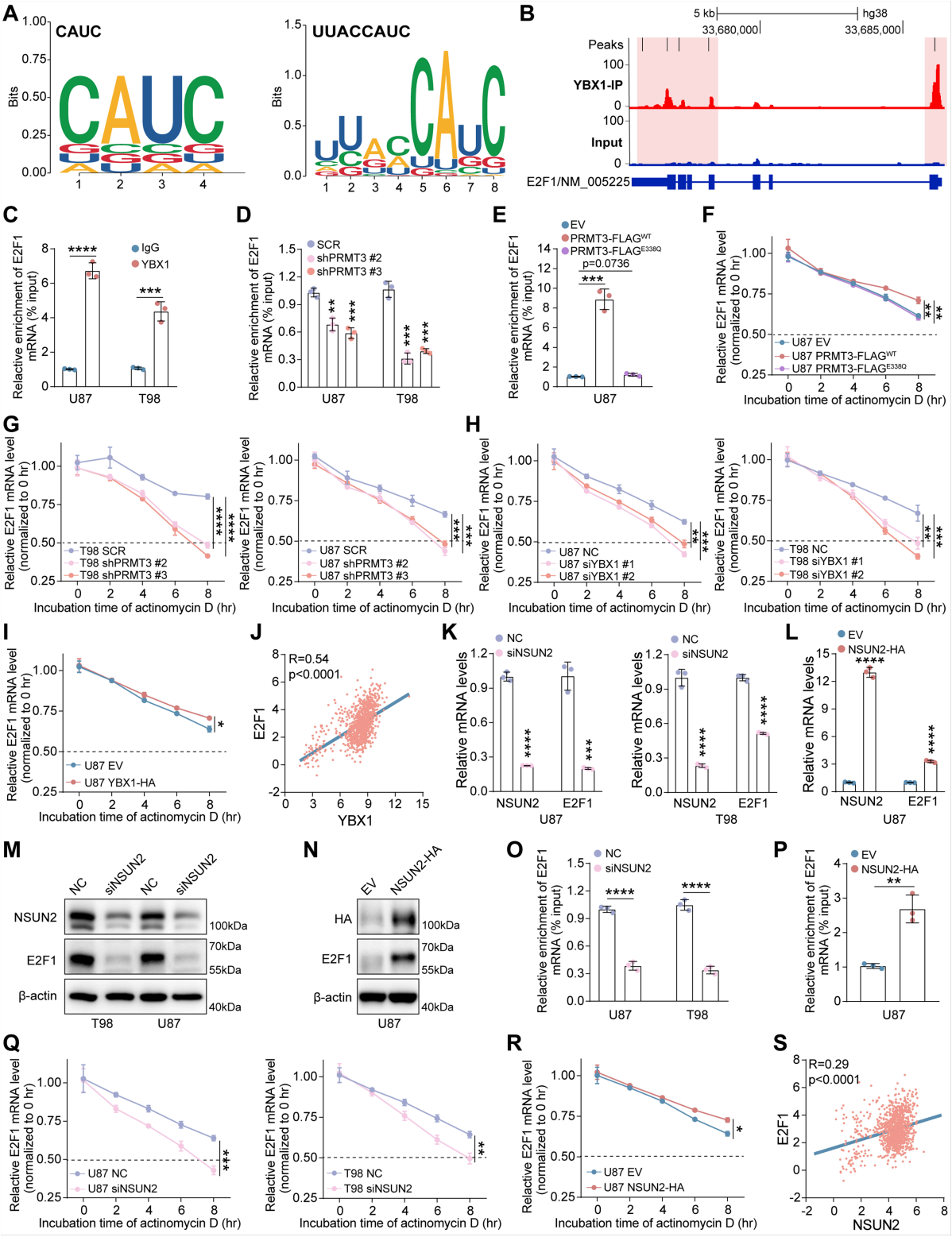


Figure 7

PRMT3-YBX1 axis enhances the stabilization of m5C-modified E2F1 mRNA. A De novo motif analysis of the top 2,000 YBX1 eCLIP seq peaks using HOMER (v4.11.2), showing the top-ranked 4 bp motif (left) and the top-ranked motif of 8 bp (right). **B** IGV tracks of YBX1 eCLIP-seq and input control profiles across the E2F1 transcriptional locus. **C** Validation of the interaction between YBX1 protein and E2F1 mRNA in U87 and T98 cells by RIP assay. IgG served as a negative control. **D**, **E** RIP-qPCR assays (by anti-YBX1

antibody) were performed in U87 and T98 cells with PRMT3 knockdown (**D**), or in U87 cells overexpressing PRMT3-WT or PRMT3-E338Q (**E**). **F-I** Cells were treated with Actinomycin D for the indicated times (0, 2, 4, 6, 8 hours). E2F1 mRNA half-life was measured by RT-qPCR in U87 cells with PRMT3 or YBX1 overexpression (**F**, **I**), U87 and T98 cells with PRMT3 or YBX1 knockdown (**G**, **H**). **J** Pearson correlation analysis of E2F1 and YBX1 expression in glioma patients from the CGGA dataset. **K-N** E2F1 mRNA (**K**, **L**) and protein (**M**, **N**) levels were assessed by RT-qPCR and western blotting in U87 and T98 cells with NSUN2 knockdown (**K**, **M**) or in U87 cells with NSUN2 overexpression (**L**, **N**). **O**, **P** RIP-qPCR assays (by anti-YBX1 antibody) were performed to assess YBX1 enrichment on E2F1 mRNA in GBM cells with NSUN2 knockdown (**O**) or overexpression (**P**). **Q**, **R** Actinomycin D chase assays were performed to determine E2F1 mRNA half-life in GBM cells with NSUN2 knockdown (**Q**) or overexpression (**R**). **S** Pearson correlation analysis of E2F1 and NSUN2 expression in glioma patients from the CGGA dataset. Data are presented as mean ± SD. **P* < 0.05, ***P* < 0.01, ****P* < 0.001, ****P*< 0.0001, n.s, not significant, versus the indicated groups, Student's t-test.

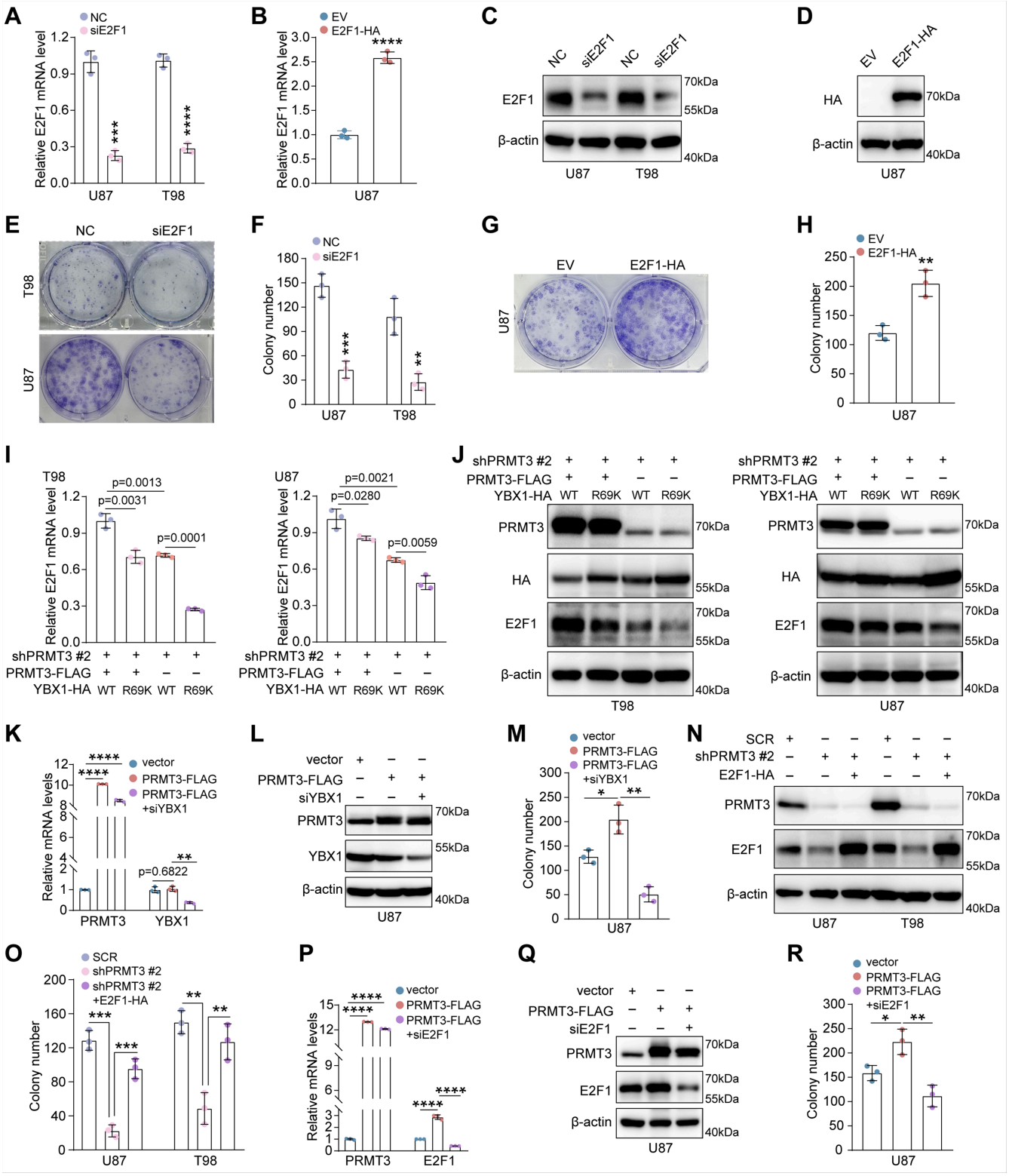


Figure 8

The effect of PRMT3-YBX1 on GBM cell proliferation is dependent on E2F1. A-D Validation of E2F1 knockdown and overexpression efficiency. E2F1 mRNA levels (**A**, **B**) and protein levels (**C**, **D**) were assessed by RT-qPCR and western blotting in U87 and T98 cells transfected with E2F1 siRNA (**A**, **C**) or in U87 cells transfected with E2F1 overexpression plasmids (**B**, **D**). **E-H** Representative images (**E**, **G**) and quantification (**F**, **H**) of colony formation assays in U87 and T98 cells upon PRMT3 knockdown or in U87

cells overexpressing PRMT3. **I**, **J** RT-qPCR (**I**) and immunoblotting (**J**) analysis of E2F1 levels in PRMT3-knockdown cells rescued with YBX1-WT or YBX1-R69K, in the presence or absence of PRMT3 re-expression. **K**, **L** Validation of YBX1 mRNA and protein levels in a PRMT3-overexpression background. U87 cells overexpressing PRMT3 with or without siRNA-mediated YBX1 knockdown were analyzed by RT-qPCR (**K**) and western blotting (**L**). **M** Quantification of colony formation assays in U87 cells overexpressing PRMT3 with or without YBX1 knockdown. **N** Validation of E2F1 protein levels in a PRMT3-knockdown background. U87 and T98 cells silencing PRMT3 with or without E2F1 overexpression were analyzed by western blotting. **O** Quantification of colony formation assays in U87 and T98 cells silencing PRMT3 with or without E2F1 overexpression. **P**, **Q** Validation of E2F1 mRNA and protein levels in a PRMT3-overexpression background. U87 cells overexpressing PRMT3 with or without siRNA-mediated E2F1 knockdown were analyzed by RT-qPCR (**P**) and immunoblotting (**Q**). **R** Quantification of colony formation assays in U87 cells overexpressing PRMT3 with or without E2F1 knockdown. Data are presented as mean ± SD. *P < 0.05, **P < 0.01, ***P < 0.001, ***P < 0.0001, versus the indicated groups, Student's t-test.

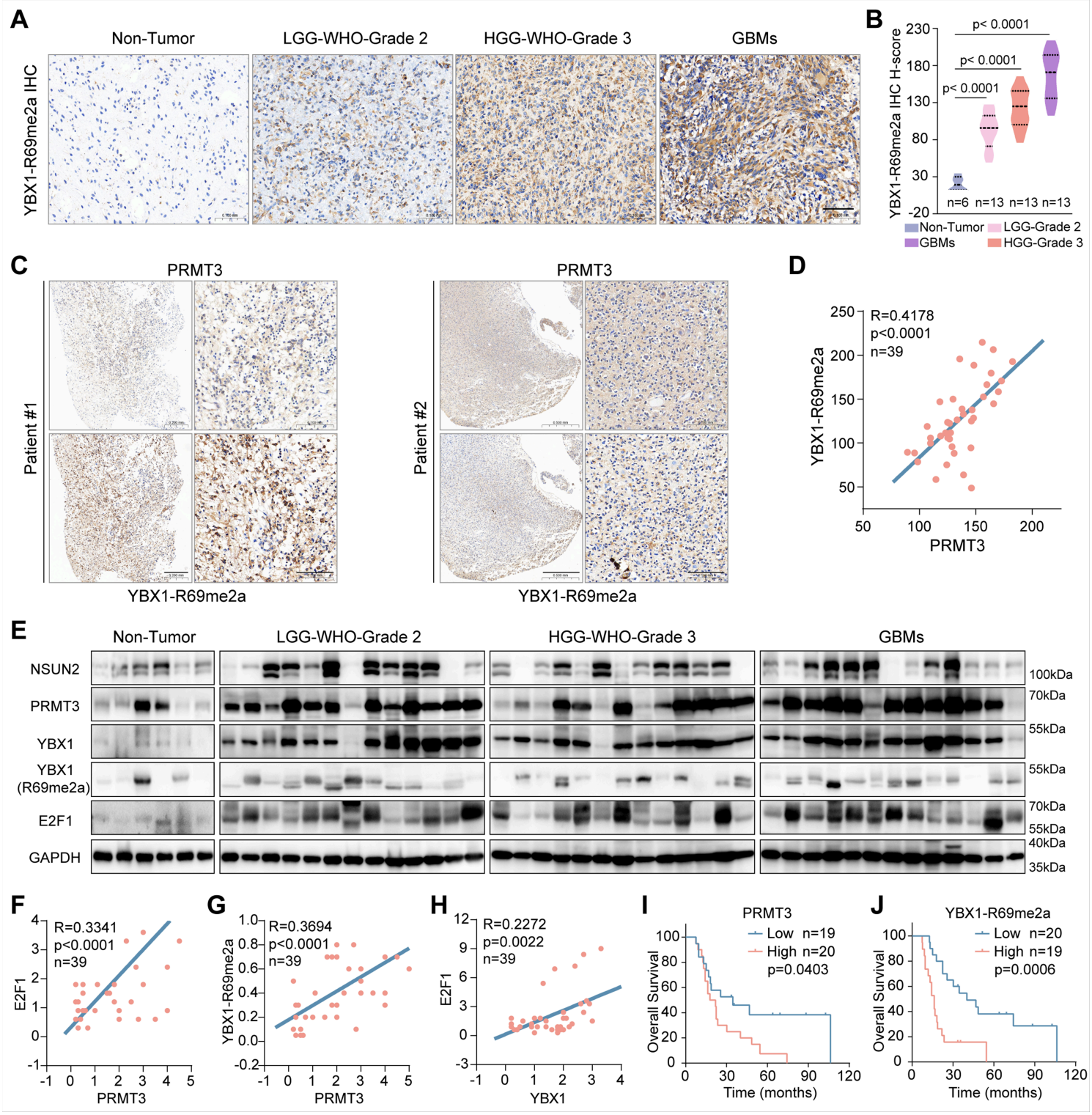


Figure 9

YBX1 is hypermethylated by PRMT3 at R69 in human glioma tissues and predicts poor patient prognosis. A, **B** Representative IHC images of YBX1-R69me2a in non-tumor brain tissue, LGG (WHO grade 2), HGG (WHO grade 3) and GBM samples (**A**). Scale bar, 100 μm. Quantitative analysis of the H-score for YBX1-R69me2a across the indicated groups (**B**). **C**, **D** Representative IHC staining of PRMT3 and YBX1-R69me2a on serial sections from the same tumor region (**C**). Scale bar, 100 μm. Correlation analysis between PRMT3 and YBX1-R69me2a IHC scores across 39 glioma specimens (**D**). **E-H**

Immunoblotting analysis of NSUN2, PRMT3, YBX1, YBX1-R69me2a, and E2F1 expression in glioma tissues (n=39) and non-tumor brain tissues (n=6) (**E**). Analysis of correlations between PRMT3 and E2F1 (**F**), PRMT3 and YBX1-R69me2a (**G**), as well as YBX1 and E2F1 (**H**) based on western blotting quantitative results from 39 glioma samples. **I**, **J** Kaplan-Meier analysis of overall survival in glioma patients based on PRMT3 (**I**) or YBX1-R69me2a levels (**J**) IHC staining intensity. Data are presented as mean ± SD. Statistical significance was determined using Student's t-test (**B**), Pearson correlation analysis (**D**, **F-H**), or the Log-rank test (**I**, **J**).

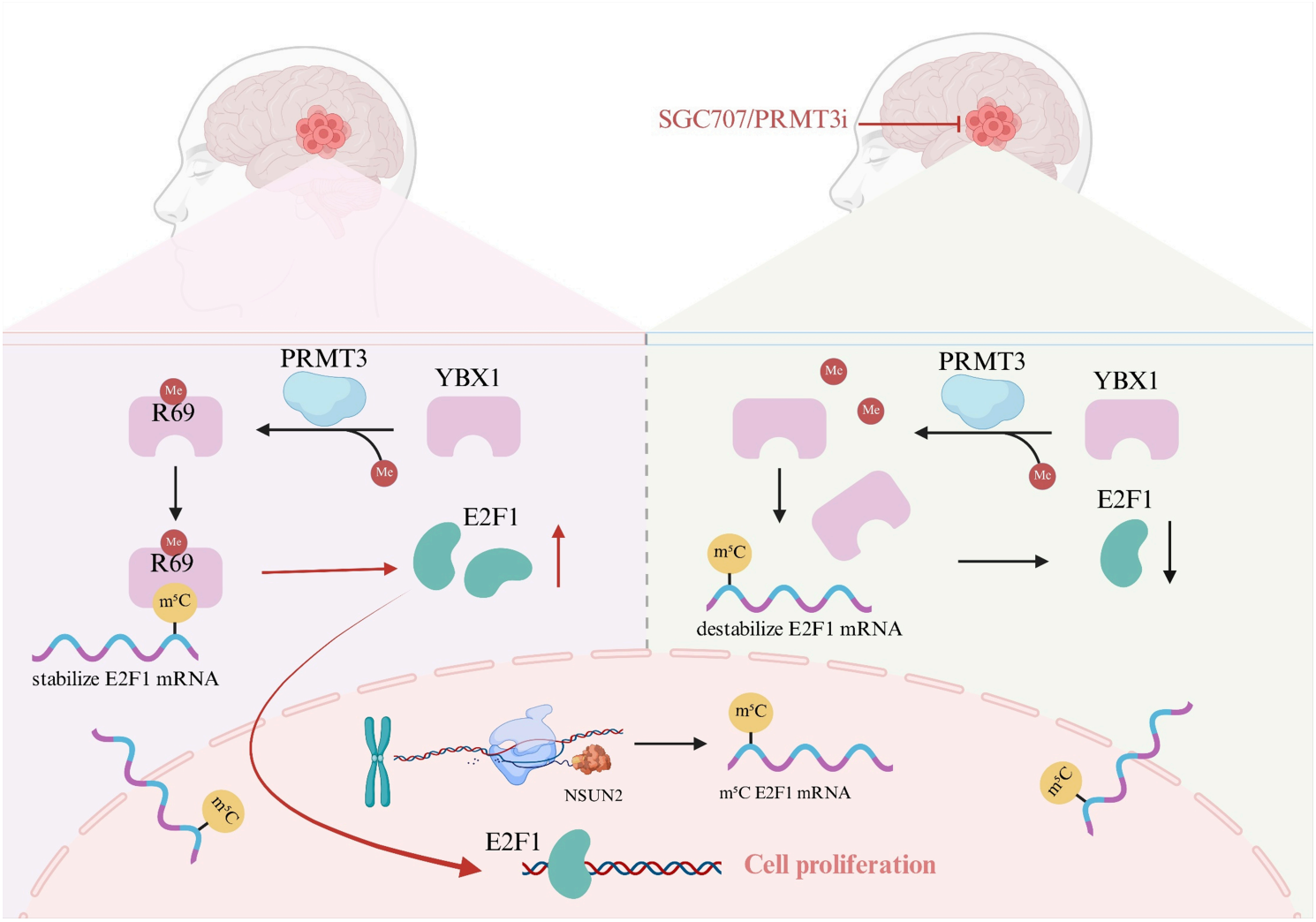


Figure 10

Schematic diagram of the mechanism by which PRMT3 promotes tumorigenesis in GBM. PRMT3 catalyzes asymmetric dimethylation of YBX1 at Arg69, which enhances the YBX1-dependent stabilization of m5C-modified E2F1 mRNA and elevates E2F1 protein expression, thereby facilitating GBM cell proliferation. SGC707 or YBX1-R69me2a peptide can inhibit GBM growth.

Supplementary Files

This is a list of supplementary files associated with this preprint. Click to download.

- Uncroppedwesternblotimages.pdf
- SupportingInformation.docx